J. Fluid Mech. (2013), *vol.* 730, *pp.* 699–732.
doi:10.1017/jfm.2013.371

Hydrodynamic diffusion of sedimenting point particles in a vertical shear flow

Andrew Crosby† and John R. Lister

Institute of Theoretical Geophysics, Department of Applied Mathematics and Theoretical Physics, University of Cambridge, Wilberforce Road, Cambridge CB3 0WA, UK

(Received 10 January 2013; revised 18 June 2013; accepted 15 July 2013; first published online 7 August 2013)

The hydrodynamic diffusion of sedimenting point particles in a vertically sheared periodic system is investigated numerically and theoretically. In both the velocity-gradient direction and the vorticity direction, the rate of hydrodynamic diffusion is reduced as the shear rate is increased. In the velocity-gradient direction, two-particle interactions cause no net displacement, and three-particle interactions are necessary for diffusive behaviour. In contrast to an unsheared system, the resulting diffusion coefficient is only weakly dependent upon the size of the system and $\widehat{D}_{xx} \sim 4.2 \times 10^{-4} n^2 (f/\mu)^4 \dot{\gamma}^{-3} \ln(0.42\widehat{L}(\mu\dot{\gamma}/f)^{1/2})$, where n is the particle number density, f the force per particle, μ the fluid viscosity, $\dot{\gamma}$ the imposed shear rate, and $\widehat{L}$ the system size. In the vorticity direction, although individual two-particle interactions cause no net displacement, a superposition of interactions is sufficient to cause diffusion-like linear growth of the ensemble-averaged square particle displacements. The associated diffusion coefficient is given by $\widehat{D}_{yy} \sim 9.47 \times 10^{-4} n (f/\mu)^2 \widehat{L} \dot{\gamma}^{-1}$. At sufficiently long times, the effect of multi-particle interactions cannot be neglected and there is a transition to another regime in which the diffusion coefficient is similar in form, but slightly reduced from this value. The dependence of $\widehat{D}_{xx}$ and $\widehat{D}_{yy}$ on the number density and dimensionless shear rate is explained using theoretical scaling arguments and analyses.

Key words: suspensions, low-Reynolds-number flows, particle/fluid flows

1. Introduction

Viscous sedimentation of particles has been the focus of much research dating back to Smoluchowski (1913), who considered the mean settling velocity of spheres within a closed container. A significant step forward was taken by Batchelor (1972), who showed how to handle the divergent integrals arising in such problems. The volume of continued research since then is evidence both of the importance of sedimentation problems, and of the complex and subtle physical processes involved. A recent review of some of the issues can be found in Guazzelli & Hinch (2011).

An important process in sedimenting suspensions is hydrodynamic diffusion since it leads to the mixing of particles within the suspension. Hydrodynamic diffusion arises from statistical fluctuations in the particle number density within the suspension

† Email address for correspondence: lister@damtp.cam.ac.uk

which drive random velocity fluctuations. It was first observed experimentally by Davis & Hassen (1988), who analysed the spreading front at the top of a sedimenting suspension, and was further analysed by Ham & Homsy (1988), who investigated hydrodynamic diffusion within the bulk of the suspension. More recently there have been further experimental investigations by Nicolai *et al.* (1995) and Nicolai & Guazzelli (1995). These experiments were complemented by numerical simulations and modelling (see e.g. Ladd 1993; Koch 1994; Cunha *et al.* 2002; Mucha & Brenner 2003). All these studies have one thing in common: they consider hydrodynamic diffusion within systems where the statistically averaged velocity (including both particles and the surrounding fluid) is uniform in space.

The aim of this paper is to investigate hydrodynamic diffusion in a system of sedimenting particles where the statistically averaged velocity is not uniform in space, which occurs in a number of different scenarios. It occurs when a suspension sediments in a closed container and the particle probability distribution has horizontal variations, most notably in the Boycott effect (Boycott 1920). It also occurs in unconfined geometries where a region of sedimenting particles, such as a spherical cloud or a cylindrical plume, generates its own large-scale flow: for a spherical cloud of particles (Nitsche & Batchelor 1997; Machu *et al.* 2001; Ekiel-Jeżewska, Metzger & Guazzelli 2006; Metzger, Nicolas & Guazzelli 2007), hydrodynamic diffusion across the statistically averaged streamlines determines the rate at which particles are lost into the tail behind the sphere; for a cylindrical plume (Pignatel *et al.* 2009; Crosby & Lister 2012), hydrodynamic diffusion determines the rate at which the plume spreads radially. Finally, it occurs in any suspension with an imposed background flow.

The system analysed here is that of a dilute suspension of very small particles sedimenting in the presence of a background linear vertical shear flow. Insights from the physical processes present in this simple system ought to be applicable to a much wider range of flows. Our chosen system is arguably the simplest system in which to consider the coupling between a large-scale flow and hydrodynamic particle interactions, yet, even for this simple system, we find some surprising and subtle results that are not what might have been expected from a simple generalization of the arguments for an unsheared suspension.

It is worth emphasizing that this system is fundamentally different from that of a sheared suspension of neutrally buoyant finite-sized particles (see e.g. Eckstein, Bailey & Shapiro 1977; Acrivos *et al.* 1992; Sierou & Brady 2004). In that system, finite-size effects are necessary to cause displacements of the particle positions as they are sheared past each other. By contrast, in the system considered here, displacements to the particle positions are instead caused by buoyancy-induced interactions between the particles, which persist even in the limit of zero particle size. There is a common point of interest: in both systems, the symmetry of two-particle interactions means that they cause no net horizontal displacement, and this plays an important role in the scaling of the hydrodynamic diffusion coefficients.

The layout of this paper is as follows. In § 2 we give the governing equations for point particles sedimenting within a vertically sheared periodic system. In § 3 we describe a numerical method of solution and present numerical calculations of the horizontal components of hydrodynamic diffusion for a range of system sizes and background shear strengths. In § 4 we use simple scaling arguments to examine how strong the background shear must be in order for the system to behave differently from an unsheared system. In § 5 we consider strongly sheared systems and approximate the particle trajectories by including only two-particle interactions in order to obtain leading-order approximations to the diffusion coefficients. This section also includes

a discussion on the form of two-particle interactions, and explains why the lack of a net horizontal displacement does not prevent diffusion-like linear growth of the ensemble-averaged square displacements in the vorticity direction. The effect of multi-particle interactions is considered in § 6. We first develop a scaling argument based on three-particle interactions for the diffusivity in the velocity-gradient direction. We also demonstrate that the leading-order two-particle approximation for displacements in the vorticity direction breaks down at very long times since the effect of multi-particle interactions can no longer be neglected.

2. Problem description

We consider a collection of N particles sedimenting within a Newtonian fluid of viscosity μ. Let the geometry be triply periodic with periods $\boldsymbol{a}_1$, $\boldsymbol{a}_2$ and $\boldsymbol{a}_3$; thus a particle with position $\boldsymbol{x}$ has periodic images at $\boldsymbol{x}+\boldsymbol{p}$, where $\boldsymbol{p}=p_1\boldsymbol{a}_1+p_2\boldsymbol{a}_2+p_3\boldsymbol{a}_3$ and $(p_1,p_2,p_3)\in\mathbb{Z}^3$. Each particle is modelled as a point force $f\boldsymbol{e}_z$ in the vertical direction, and its position evolves according to

$$\boldsymbol{u}_i(t)=\sum_{\boldsymbol{p}}\sum_{j=1}^{N} f\boldsymbol{e}_z\cdot\boldsymbol{J}(\boldsymbol{x}_j-\boldsymbol{x}_i+\boldsymbol{p})+\boldsymbol{u}^b(\boldsymbol{x}_i), \tag{2.1}$$

where

$$\boldsymbol{J}(\boldsymbol{x})\equiv\frac{1}{8\pi\mu}\left(\frac{\boldsymbol{I}}{|\boldsymbol{x}|}+\frac{\boldsymbol{x}\boldsymbol{x}}{|\boldsymbol{x}|^3}\right) \tag{2.2}$$

is the Oseen tensor, $\boldsymbol{u}^b(\boldsymbol{x})$ is an applied background flow, and the self-induced contribution from $j=i$ and $\boldsymbol{p}=\boldsymbol{0}$ is excluded from the sum. The infinite sum in (2.1) is formally divergent; the divergence arises because the density of the suspension as a whole is different to that of the ambient fluid. However, as shown by Hasimoto (1959), this density contrast can be balanced by a global pressure gradient, the inclusion of which removes the divergence and allows (2.1) to be evaluated. The conditions under which finite-sized particles can be approximated as point forces are discussed in appendix B.

We focus on the case where the applied flow is a vertical shear flow of strength $\dot\gamma$, with velocity gradient in the x-direction (and thus vorticity in the y-direction):

$$\boldsymbol{u}^b(\boldsymbol{x})=\dot\gamma(\boldsymbol{x}\cdot\boldsymbol{e}_x)\boldsymbol{e}_z. \tag{2.3}$$

The periodic geometry is also sheared by the background flow. For the initial geometry we choose a periodic cube of side $\widehat{L}$ such that the periodic lattice vectors are given by

$$\boldsymbol{a}_1(t)=\widehat{L}(\boldsymbol{e}_x+\dot\gamma t\boldsymbol{e}_z),\quad \boldsymbol{a}_2=\widehat{L}\boldsymbol{e}_y,\quad \boldsymbol{a}_3=\widehat{L}\boldsymbol{e}_z. \tag{2.4}$$

The spatially periodic geometry is also periodic in time with period $\dot\gamma^{-1}$ since $\boldsymbol{a}_1(t+\dot\gamma^{-1})=\boldsymbol{a}_1(t)+\boldsymbol{a}_3$, as shown in figure 1.

By grouping together the velocities induced by any particle and all its periodic images, the velocity (2.1) of a particular particle can be rewritten as

$$\boldsymbol{u}_i(t)=\sum_{j\neq i}\boldsymbol{u}^p(\boldsymbol{x}_j-\boldsymbol{x}_i,\dot\gamma t)+\boldsymbol{u}^s(\dot\gamma t)+\boldsymbol{u}^b(\boldsymbol{x}_i), \tag{2.5}$$

where $\boldsymbol{u}^p(\boldsymbol{x},\dot\gamma t)$ is the velocity induced on a particle by another particle at separation $\boldsymbol{x}$ and by all its periodic images, and $\boldsymbol{u}^s(\dot\gamma t)$ is the velocity self-induced on a particle by its own periodic images. Both $\boldsymbol{u}^p$ and $\boldsymbol{u}^s$ are functions of the structure of the periodic lattice, and hence, from (2.4), are functions of $\dot\gamma t$. Since the velocity induced

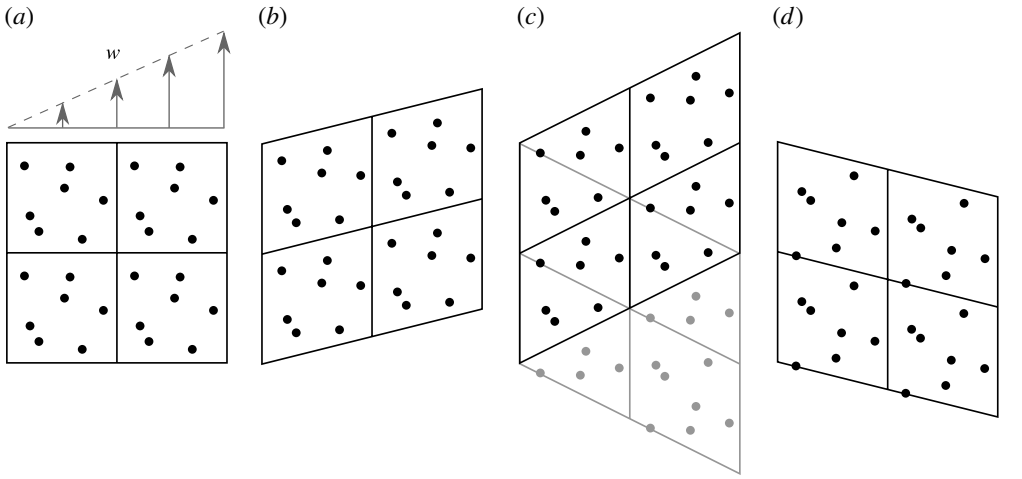

FIGURE 1. Evolution of the periodic geometry at (*a*) $\dot{\gamma}t = 0$, (*b*) $\dot{\gamma}t = 1/4$, (*c*) $\dot{\gamma}t = 1/2$ and (*d*) $\dot{\gamma}t = 3/4$. The spatially periodic lattice evolves periodically in time, with period $\dot{\gamma}^{-1}$, as demonstrated by the equivalence of the lattice vectors for $\dot{\gamma}t = 1/2$ and $\dot{\gamma}t = -1/2$ shown in (*c*).

by a particle's own images is exactly the same for all particles, $\boldsymbol{u}^s(\dot{\gamma}t)$ has no effect on the dynamics of the system apart from causing a periodic displacement to all the particle positions as they are sheared past their own images. We can thus neglect $\boldsymbol{u}^s$ in the subsequent theoretical analysis without affecting the coefficients of hydrodynamic diffusion.

We assume that at $t = 0$ the particles are distributed randomly within the system according to a uniform probability distribution. Since a uniform probability distribution is a solution to the associated equations of probability conservation (Koch & Shaqfeh 1991), the particle distribution remains uniform for all time when averaged across the ensemble of different realizations.

We non-dimensionalize lengths by the typical inter-particle separation $l \equiv \widehat{L}N^{-1/3}$, and times by the shear time scale $\dot{\gamma}^{-1}$. We also define a dimensionless shear strength

$$\Gamma \equiv \frac{\mu}{f} l^2 \dot{\gamma}, \tag{2.6}$$

which represents the ratio of the background shear velocity to the hydrodynamic velocity induced by a single particle at a typical particle separation. Under this non-dimensionalization, the edges of the initial periodic cube have a dimensionless length $L \equiv N^{1/3}$ and, consequently, the average particle number density is unity. From this point on, all quantities are dimensionless; for simplicity, we continue to use the same notation $\boldsymbol{x}$, $\boldsymbol{u}$ and t for the dimensionless positions, velocities and times. For example, we write the particle velocity as

$$\boldsymbol{u}_i(t) = \frac{1}{\Gamma} \sum_{j \neq i} \boldsymbol{u}^p(\boldsymbol{x}_j - \boldsymbol{x}_i, t) + \frac{1}{\Gamma} \boldsymbol{u}^s(t) + \boldsymbol{u}^b(\boldsymbol{x}_i), \tag{2.7}$$

where

$$\boldsymbol{u}^b(\boldsymbol{x}) = (\boldsymbol{x} \cdot \boldsymbol{e}_x)\boldsymbol{e}_z, \quad \boldsymbol{u}^p(\boldsymbol{x}, t) = \sum_{\boldsymbol{p}} \boldsymbol{e}_z \cdot \boldsymbol{J}(\boldsymbol{x} + \boldsymbol{p}), \quad \boldsymbol{u}^s(t) = \sum_{\boldsymbol{p} \neq \boldsymbol{0}} \boldsymbol{e}_z \cdot \boldsymbol{J}(\boldsymbol{p}), \tag{2.8}$$

and

$$\boldsymbol{J}(\boldsymbol{x}) \equiv \frac{1}{8\pi}\left(\frac{\boldsymbol{I}}{|\boldsymbol{x}|} + \frac{\boldsymbol{x}\boldsymbol{x}}{|\boldsymbol{x}|^3}\right). \tag{2.9}$$

With this choice of non-dimensionalization, increasing the dimensionless shear strength Γ corresponds to decreasing the magnitude of the hydrodynamic velocities.

2.1. *Hydrodynamic diffusion*

We define $\Delta\boldsymbol{x}_i(t) \equiv \boldsymbol{x}_i(t) - \boldsymbol{x}_i(0)$ to be the displacement of a particle from its initial position. For a single realization, the mean-square particle displacements can be calculated as $N^{-1}\sum_i \Delta\boldsymbol{x}_i(t)^2$. Since the hydrodynamic velocity fluctuations in this system of sedimenting particles are dominated by fluctuations on the scale of the system (Caflisch & Luke 1985), which diverge as $L \to \infty$, we cannot obtain statistical convergence of the mean-square displacements by taking the limit of large system size $L \to \infty$ (and hence of $N \to \infty$). Instead we must average the mean-square displacements either over an ensemble of different realizations, or over many periods of time from the same realization, in order to obtain statistical convergence. Provided the system is ergodic, these two averaging methods will be equivalent.

We write the ensemble-averaged mean-square displacements as $\langle\Delta\boldsymbol{x}(t)\Delta\boldsymbol{x}(t)\rangle$. If these mean-square displacements grow linearly at large times, then we consider the motion to be diffusive with a tensor diffusion coefficient given by

$$\boldsymbol{D} \equiv \lim_{t\to\infty} \frac{1}{2}\frac{\mathrm{d}}{\mathrm{d}t}\langle\Delta\boldsymbol{x}(t)\Delta\boldsymbol{x}(t)\rangle. \tag{2.10}$$

In general, we might have expected the physical mechanism behind any linear growth in the mean-square displacements to be a random walk in the position of the particle caused by velocity fluctuations due to hydrodynamic interactions with other particles. However, linear growth of the mean-square displacements does not necessarily imply an underlying random-walk-like behaviour; indeed, we will demonstrate that there is another mechanism that produces linear growth in a sheared suspension.

Particle displacements in the z-direction are dominated by the background shear flow and do not grow diffusively. While it is still possible to define a coefficient of longitudinal diffusion by subtracting the leading-order advective effect of the background flow (see Sierou & Brady (2004) for a detailed discussion), we restrict our attention here to analysis of diffusive growth in the horizontal particle displacements. For the horizontal components of the diffusion tensor $\boldsymbol{D}$, we find that symmetry implies that $D_{xy} = D_{yx} = 0$, but D_{xx} and D_{yy} are non-zero.

3. Numerical calculations

3.1. *Method*

We evaluated the sums in (2.8) numerically via Ewald summation (Hasimoto 1959), which splits the sum up into local contributions, which are evaluated directly, and far-field contributions, which are evaluated in Fourier space. The Fourier sum was evaluated by the smooth particle-mesh method of Saintillan, Darve & Shaqfeh (2005), which uses cardinal B-splines to interpolate the point forces onto a regular grid, allowing the use of fast Fourier transforms. If the Ewald coefficient is chosen such that most particles only contribute through the Fourier sum, then this use of fast Fourier transforms allows the full sum to be evaluated efficiently in $O(N\log N)$ operations. Our numerical calculations used an Ewald coefficient $\alpha = 1.4$, a cutoff length of 2

for the direct sum, $4L$ Fourier modes for the Fourier sum, and eighth-order cardinal B-splines for interpolation.

The numerical simulations were evolved in time using a fourth-order Runge–Kutta method with a variable time step. The time step was taken to be 0.2 times the maximum strain rate between any two particles, where the strain rate between two particles is defined to be the difference in their velocities divided by their separation. The use of a high-order method and a variable time step defined in this way ensures accurate resolution of close particle interactions.

Numerical simulations were performed for periodic lengths of $L = 5$, 10, 15, 20 and 30 (hence $N = 125$–$27\,000$) and, for each length, shear strengths of $\Gamma = 0.25$, 0.5, 1, 2, 4 and 8. For each set of parameters, an ensemble average was taken over many realizations of the system, and in each case the total number of particles included in the average was at least 10^5. All the simulations were evolved up to a dimensionless time of least $t = 100$ (100 shear times), and diffusion coefficients were calculated using a least-squares linear fit to the mean-square particle displacements for $t \geqslant 20$.

Uncertainty in the numerical results might arise from one of two sources: (i) inaccuracies in the numerical calculation of particle velocities and the subsequent time-stepping; (ii) statistical uncertainty in the calculation of an ensemble average from a finite number of realizations.

To confirm that the numerically calculated velocities and the numerical time-stepper were sufficiently accurate, two ensembles of realizations for $\Gamma = 1$ and 2 and $L = 10$ were also calculated with half the time step, twice the direct-sum cutoff, and twice the number of Fourier modes. In both ensembles the diffusion coefficients were within 5 % of those calculated using the original set of numerical parameters. This slight difference is indistinguishable from the expected statistical uncertainty.

The statistical uncertainty can be estimated either from the standard deviation of the mean-square displacements of N_R different realizations scaled by $N_R^{-1/2}$ (cf. the central limit theorem), or, alternatively, from the magnitude of fluctuations about a linear fit to the ensemble-averaged mean-square displacements in the diffusive regime. The latter method is more suited to simulations with very small diffusion coefficients, for which the standard deviation of the mean-square displacements is dominated by the contribution from the initial period of ballistic growth; when applied to the results presented here, it implies statistical uncertainties of no more than 10 % in the calculated coefficients of diffusion.

The numerical inaccuracies and statistical uncertainties are sufficiently small that the results below are robust.

3.2. *Results*

The evolution of the mean-square particle displacements $\langle \Delta x^2(t) \rangle$ and $\langle \Delta y^2(t) \rangle$ for an ensemble of simulations with $L = 15$ and $\Gamma = 1$ is shown in figure 2. Both exhibit a short-time regime of quadratic (ballistic) growth, and then exhibit linear (diffusive) growth at long times. The long-time rate of growth of $\langle \Delta x^2(t) \rangle$ is much less than that of $\langle \Delta y^2(t) \rangle$, which suggests that the mechanisms behind diffusive growth in the two directions is different.

To investigate the dependence of the diffusion coefficients on the shear strength Γ, D_{xx} and D_{yy} are plotted against Γ in figure 3. In both cases, the coefficients decrease as Γ is increased, but D_{xx} decreases much more rapidly. For large Γ, D_{yy} shows a clear Γ^{-2} scaling, whereas the scaling of D_{xx} is somewhere between Γ^{-3} and Γ^{-4}. Note that the choice of non-dimensionalization by the shear time scale introduces a factor of Γ^{-1} into each of these scalings that would not have been present if we

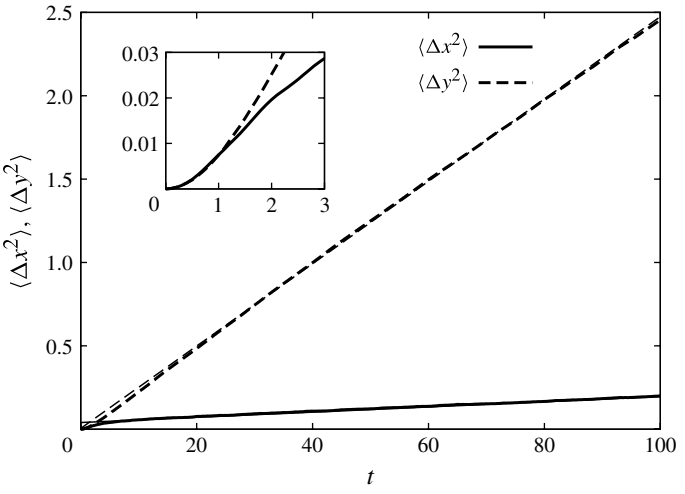

FIGURE 2. Evolution of the mean-square particle displacements $\langle \Delta x^2(t) \rangle$ and $\langle \Delta y^2(t) \rangle$ for an ensemble of simulations with $L = 15$ and $\Gamma = 1$ (heavy lines). After an initial transient, both mean-square displacements exhibit linear growth. The linear least-squares fits for $20 \leqslant t \leqslant 100$ (thin lines) are almost indistinguishable, and give values for the diffusivities of $D_{xx} = 7.76 \times 10^{-4}$ and $D_{yy} = 1.23 \times 10^{-2}$. A close-up of the early-time ballistic growth is shown in the inset.

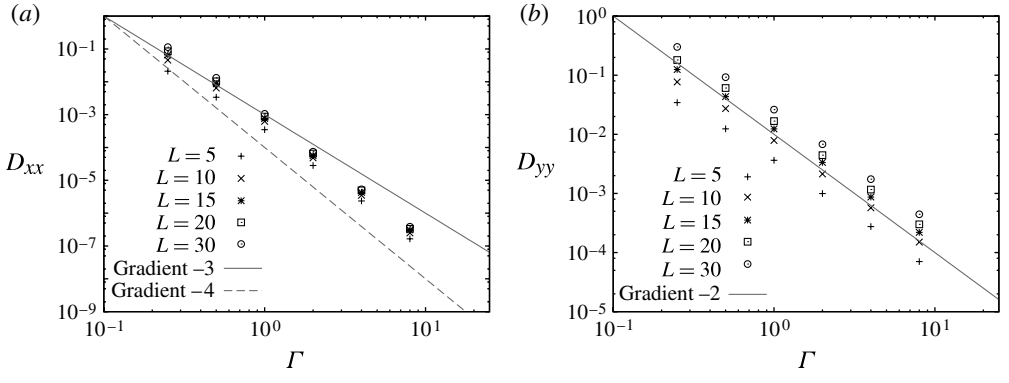

FIGURE 3. (*a*) Variation of D_{xx} with shear strength Γ. For comparison, scalings of Γ^{-3} and Γ^{-4} are also shown (grey lines); the variation of D_{xx} falls somewhere between the two. (*b*) Variation of D_{yy} with shear strength Γ. For comparison, a scaling of Γ^{-2} is also shown (grey line), which is a good match to the variation of D_{yy} for large Γ.

had instead non-dimensionalized by a time scale based on hydrodynamic interactions. Consequently, if we return to dimensional variables, these observations correspond to scalings with the dimensional shear rate $\dot{\gamma}$ of $\dot{\gamma}^{-1}$ for $\widehat{D}_{yy}$ and between $\dot{\gamma}^{-2}$ and $\dot{\gamma}^{-3}$ for $\widehat{D}_{xx}$. In both cases, the dimensional diffusion coefficients tend to zero as the strength of the background shear flow is increased.

The variation of the (dimensionless) diffusion coefficients with L is shown in figure 4. There is an approximately linear growth of D_{yy} with L, but the growth of D_{xx} with L is sub-linear.

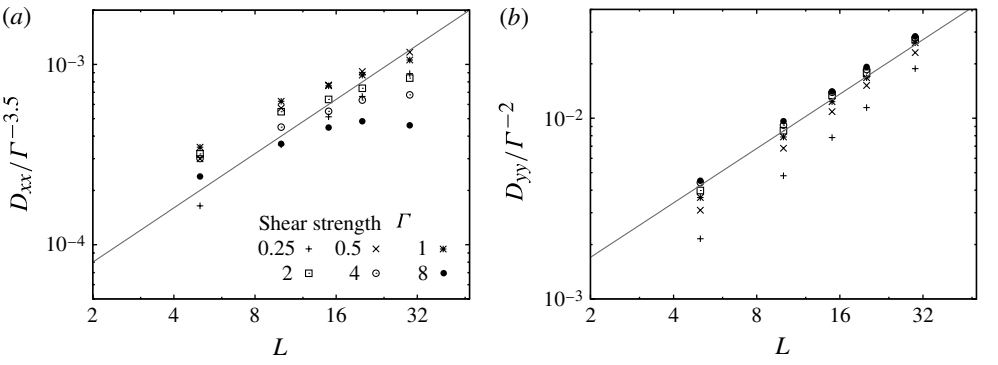

FIGURE 4. (*a*) Variation of $D_{xx}/\Gamma^{-3.5}$ with system size L. The line shows a linear variation for comparison. While D_{xx} increases with L, the rate of increase is sub-linear. (*b*) Variation of D_{yy}/Γ^{-2} with system size L. A linear variation with L (grey line) is a good match to the variation of D_{yy} for the larger values of Γ. In both directions, the scaling $D \propto L^{3/2}$ of Koch (1994) would be recovered in the limit $\Gamma \to 0$.

In summary, we deduce from the numerical results that D_{yy} shows a $L\Gamma^{-2}$ scaling, whereas the variation of D_{xx} with Γ and L cannot be captured by a simple power-law scaling.

Motivated by the theoretical analysis in § 6.2, we also investigated the very long time ($t \gg L^{1/2}\Gamma$) behaviour of the mean-square displacements in the y-direction and found evidence of another regime with slightly reduced values of D_{yy}.

4. Simple scalings

The diffusion coefficients in an unsheared system are predicted to vary with system size according to the simple scaling law $D \propto L^{3/2}$ (Koch 1994; Cunha *et al.* 2002). We begin by rederiving this scaling and then consider how the introduction of a background shear flow influences the analysis.

When particles are distributed through a system according to a uniform probability distribution, there are statistical fluctuations about the average number density of particles between any two regions. These fluctuations cause differences in the average density between the two regions, which in turn drive hydrodynamic velocity fluctuations. The largest velocity fluctuations arise from the system-scale density fluctuations (Caflisch & Luke 1985) which generate a typical dimensional velocity $\widehat{U}_{\widehat{L}} \sim (f/\mu)n^{1/2}\widehat{L}^{1/2}$ (Cunha *et al.* 2002). In our non-dimensionalization, this typical velocity is $U_L \sim L^{1/2}\Gamma^{-1}$. (Note that the factor Γ^{-1} only appears here due to our choice of a non-dimensionalization based on the shear time scale $\dot{\gamma}^{-1}$.) For sufficiently small times, particle trajectories evolve ballistically according to the initial system-scale velocity fluctuations, leading to a quadratic growth in the mean-square particle displacement

$$\langle \Delta \boldsymbol{x}^2(t) \rangle \sim (U_L t)^2 \sim L\Gamma^{-2}t^2. \tag{4.1}$$

If rearrangement of the particles causes the density fluctuations, and hence the velocity fluctuations, to vary on a time scale T, then the quadratic ballistic growth continues for an $O(T)$ period of time.

For an unsheared system, the system-scale velocity fluctuations drive a convective motion and the velocity fluctuations vary on a time scale $T_L \sim L/U_L \sim L^{1/2}\Gamma$ that corresponds to the overturning time of a system-scale convection cell. The random nature of the fluctuations leads to diffusive growth of the particle displacements for $t \gg T_L$ with a diffusion coefficient

$$D \sim U_L^2 T_L \sim L^{3/2}\Gamma^{-1}. \tag{4.2}$$

In contrast, the addition of a background shear flow shears out the system-scale density fluctuations on a time scale $T_\Gamma \sim 1$. The critical parameter that determines whether velocity fluctuations vary on the convective time scale T_L or the shear time scale T_Γ is the dimensionless ratio $S \equiv L/U_L = L^{1/2}\Gamma$ between the shear velocity and the hydrodynamic velocity fluctuations on the scale of the system. If $S \ll 1$, then hydrodynamic velocity fluctuations are dominant, implying that $T_L \ll T_\Gamma$, and we expect (4.2) to hold. If $S \gg 1$, then the background shear is dominant, implying that $T_\Gamma \ll T_L$, and velocity fluctuations will vary in an $O(T_\Gamma)$ time (although their typical magnitude will remain the same). It is tempting at this stage to simply replace the time scale T_L by T_Γ in (4.2) to predict that for a strongly sheared system ($S \gg 1$)

$$D \sim U_L^2 T_\Gamma \sim L\Gamma^{-2}. \tag{4.3}$$

The prediction (4.3) agrees with the scaling that we found numerically for D_{yy} in the previous section, but it does not agree with the scaling for D_{xx}, which suggests that this simple scaling argument based on T_Γ is missing an important physical idea. The missing idea is that two-particle interactions in a vertical shear flow cause no net horizontal displacement, and, as the following sections will reveal, the simple scaling argument does not even give the correct explanation for the $L\Gamma^{-2}$ scaling of D_{yy}.

5. Two-particle interactions at large shear strengths

If the shear strength is infinite ($\Gamma = \infty$), then hydrodynamic interactions between particles are negligible, and the particles are simply advected along straight lines by the background shear flow. In this case, there can be no hydrodynamic diffusion. For large, but finite, shear strength, the hydrodynamic interactions between particles will cause small perturbations to the straight infinite-shear-rate trajectories. In this case, we can perform a perturbation analysis about the infinite-shear-rate trajectories to determine the leading-order effect of horizontal perturbations due to two-particle interactions.

5.1. *Perturbation analysis for* $\Gamma \gg 1$

For $\Gamma \gg 1$, we write the trajectory of particle i as

$$\boldsymbol{x}_i(t) = \boldsymbol{x}_i^0(t) + \Gamma^{-1}\boldsymbol{x}_i^1(t) + O(\Gamma^{-2}), \tag{5.1}$$

where $\boldsymbol{x}_i^0(t)$ is the straight infinite-shear-rate trajectory and $\boldsymbol{x}_i^1(t)$ is a small first-order correction due to hydrodynamic interactions (figure 5). The velocity of particle i is given by (2.7), which, neglecting the periodic contribution from the particle's own images, is

$$\boldsymbol{u}_i(t) = \boldsymbol{u}^b(\boldsymbol{x}_i) + \Gamma^{-1}\sum_{j\neq i}\boldsymbol{u}^p(\boldsymbol{x}_j - \boldsymbol{x}_i, t). \tag{5.2}$$

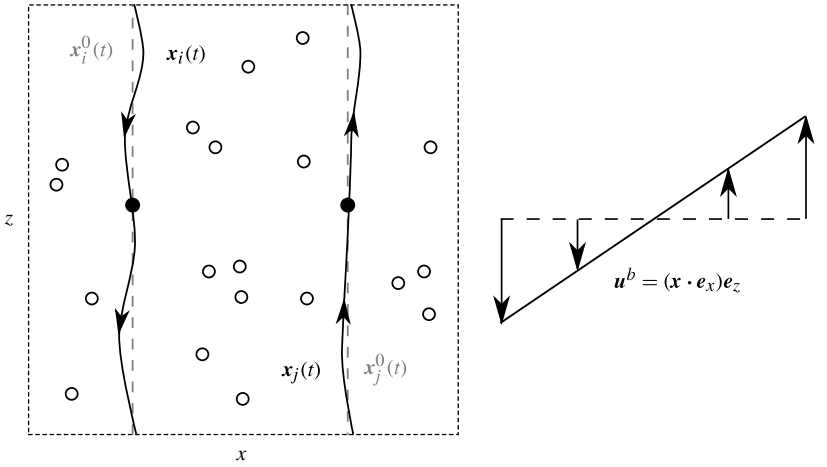

FIGURE 5. When the system is strongly sheared ($\Gamma \gg 1$), the relative motion of two particles can be closely approximated by replacing the actual trajectories $\boldsymbol{x}_i(t)$ and $\boldsymbol{x}_j(t)$ (curves) by vertical straight lines $\boldsymbol{x}_i^0(t)$ and $\boldsymbol{x}_j^0(t)$ (dashed lines).

Substituting (5.1) in (5.2), we expand the particle's velocity as

$$\boldsymbol{u}_i(t) = (\boldsymbol{x}_i^0 \cdot \boldsymbol{e}_x)\boldsymbol{e}_z + \Gamma^{-1}\left((\boldsymbol{x}_i^1 \cdot \boldsymbol{e}_x)\boldsymbol{e}_z + \sum_{j\neq i} \boldsymbol{u}^p(\boldsymbol{x}_j^0 - \boldsymbol{x}_i^0, t)\right) + O(\Gamma^{-2}). \tag{5.3}$$

Since the hydrodynamic velocities are already $O(\Gamma^{-1})$, replacing the actual particle positions by their leading-order approximations in the argument of $\boldsymbol{u}^p$ gives rise to only an $O(\Gamma^{-2})$ correction.

At leading order, we recover the infinite-shear-rate trajectory

$$\boldsymbol{x}_i^0(t) = \boldsymbol{x}_i(0) + t(\boldsymbol{x}_i(0) \cdot \boldsymbol{e}_x)\boldsymbol{e}_z, \tag{5.4}$$

which is simply a straight vertical path.

Equating terms of order Γ^{-1} in (5.3), we find that the first-order corrections satisfy

$$\frac{\mathrm{d}\boldsymbol{x}_i^1}{\mathrm{d}t} = \sum_{j\neq i} \boldsymbol{u}^p(\boldsymbol{x}_{ij}^0(t), t) + (\boldsymbol{x}_i^1 \cdot \boldsymbol{e}_x)\boldsymbol{e}_z, \tag{5.5}$$

where $\boldsymbol{x}_{ij} = \boldsymbol{x}_j - \boldsymbol{x}_i$ denotes the separation between particles i and j. Equation (5.5) can be interpreted as the sum of $N-1$ independent two-particle interactions.

The leading-order horizontal displacements are found by integrating (5.5) with respect to t to obtain

$$\boldsymbol{x}_i^{1H}(t) = \sum_{j\neq i} \boldsymbol{X}_L^H(\boldsymbol{x}_{ij}(0), t), \tag{5.6}$$

where

$$\boldsymbol{X}_L^H(\boldsymbol{x}, t) \equiv \int_0^t \boldsymbol{u}^{p\,H}(\boldsymbol{x} + \hat{t}(\boldsymbol{e}_x \cdot \boldsymbol{x})\boldsymbol{e}_z, \hat{t})\,\mathrm{d}\hat{t} \tag{5.7}$$

denotes the (scaled) horizontal displacement due to a single two-particle interaction between particles with an initial separation $\boldsymbol{x}$. We use the superscript H to designate

the horizontal components of a vector, and the subscript L to emphasize that the periodic velocities $\boldsymbol{u}^{p\,H}$, and hence also $\boldsymbol{X}_L^H$, depend on the size of the system.

This perturbation analysis for $\Gamma \gg 1$ is valid provided the perturbations $\Gamma^{-1}\boldsymbol{x}_i^1$ to the infinite-shear-rate trajectory remain sufficiently small. More explicitly, the expansion used to obtain (5.3) requires these perturbations to be small compared to the separation between particle i and the other particles in the sum. Since these perturbations grow with time (figure 2), albeit slowly for $\Gamma \gg 1$, we can see that the expansion will eventually break down for sufficiently large t at fixed Γ. However, for a fixed value of t, the expansion

$$\boldsymbol{x}_i(t) \sim \boldsymbol{x}_i^0(t) + \Gamma^{-1}\boldsymbol{x}_i^1(t) \tag{5.8}$$

will be asymptotically correct as $\Gamma \to \infty$.

The hydrodynamic diffusion coefficients depend on the ensemble-averaged mean-square displacements. From (5.1) the horizontal displacements satisfy

$$\langle \Delta\boldsymbol{x}^H(t)^2\rangle = \Gamma^{-2}\langle \boldsymbol{x}^{1H}(t)^2\rangle + O(\Gamma^{-3}). \tag{5.9}$$

Again, we expect this expression to be asymptotically correct as $\Gamma \to \infty$ for a fixed value of t. The behaviour as $t \to \infty$ is less apparent, which we will return to in § 6.2.

To calculate the ensemble average in (5.9), we note that, because the $N-1$ contributions in (5.6) are independent, the ensemble average is equivalent to an integral over the periodic box of all possible initial particle separations. Thus

$$\langle \boldsymbol{x}^{1H}(t)^2\rangle = \frac{N-1}{L^3}\int_{V(L)} \boldsymbol{X}_L^H(\boldsymbol{x}', t)^2\,\mathrm{d}^3\boldsymbol{x}', \tag{5.10}$$

where $V(L)$ is a single copy of the periodic box.

The dependence of (5.10) on L can be made explicit by noting that $(N-1)/L^3 \approx 1$ for a system of many particles, and by making the change of variables $\tilde{\boldsymbol{x}} = \boldsymbol{x}'/L$. The change of variables produces a factor of L^3 from the volume of integration and two factors of L^{-1} from the dependence of the hydrodynamic velocities, and hence of $\boldsymbol{X}_L^H$, on the inverse separation between particles through (2.9). Thus

$$\langle \boldsymbol{x}^{1H}(t)^2\rangle = L\int_{V(1)} \boldsymbol{X}_1^H(\tilde{\boldsymbol{x}}, t)^2\,\mathrm{d}^3\tilde{\boldsymbol{x}}. \tag{5.11}$$

The linear dependence of $\langle \boldsymbol{x}^{1H}(t)^2\rangle$ on L in (5.11) implies that the leading-order horizontal displacements are dominated by two-particle interactions on the scale of the system.

Since $\langle \boldsymbol{x}^{1H}(t)^2\rangle$ is dominated by the system-scale interactions, the leading-order approximation in (5.9) should be accurate provided only that Γ is sufficiently large that the perturbation analysis accurately approximates these system-scale interactions. Thus we expect only to require $S = L^{1/2}\Gamma \gg 1$ (slightly weaker than the initial assumption $\Gamma \gg 1$) so that on the scale of the system the shear flow is strong relative to hydrodynamic velocity fluctuations.

Numerical evaluation of $\langle x^1(t)^2\rangle$ and $\langle y^1(t)^2\rangle$ from (5.11) is shown in figure 6. At short times, both $\langle x^1(t)^2\rangle$ and $\langle y^1(t)^2\rangle$ exhibit the expected ballistic growth. At long times, $\langle y^1(t)^2\rangle$ exhibits a diffusion-like linear growth with gradient $1.88 \times 10^{-3}L$, whereas $\langle x^1(t)^2\rangle$ asymptotes to a constant value.

Combining the relationship between the diffusion coefficients $\boldsymbol{D}$ and the mean-square displacements (2.10), the leading-order approximation of the mean-square displacements (5.9), and the behaviour of this leading-order approximation (figure 6),

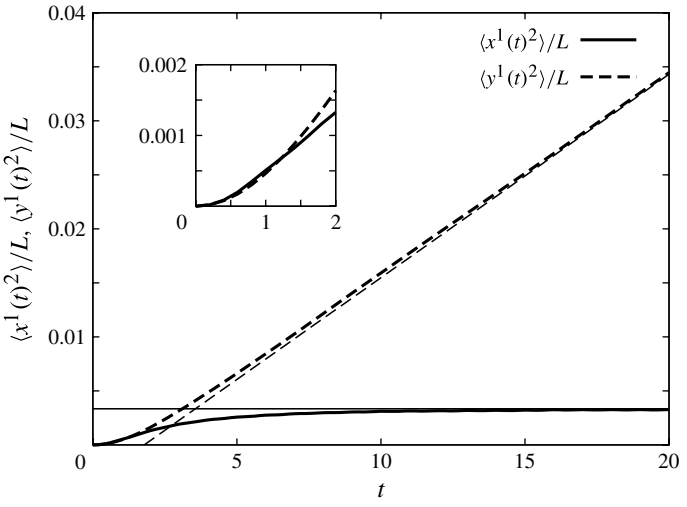

FIGURE 6. Numerical evaluation from (5.11) of the scaled mean-square displacements $\langle \boldsymbol{x}^{1H}(t)^2\rangle/L$ due to two-particle interactions (heavy lines). At short times, both $\left\langle x^1(t)^2\right\rangle/L$ and $\left\langle y^1(t)^2\right\rangle/L$ exhibit ballistic growth (inset). At longer times, $\left\langle y^1(t)^2\right\rangle/L$ grows linearly with gradient 1.88×10^{-3} (thin line), suggesting diffusive growth in the y-direction; whereas $\left\langle x^1(t)^2\right\rangle/L$ asymptotes to a constant value of 3.35×10^{-3} (thin line), implying that there is no diffusive growth in the x-direction at this order.

we predict that

$$D_{xx}\sim o(\Gamma^{-2}),\quad D_{yy}\sim 9.4\times10^{-4}L\Gamma^{-2} \tag{5.12}$$

as $S\to\infty$.

5.2. *Comparison with numerical simulations*

Figure 7 shows the scaled mean-square displacements $\langle\Delta x^2\rangle/\Gamma^{-2}$ from the full calculations with $L=15$ and various values of Γ. As Γ increases, the scaled mean-square displacements collapse onto the leading-order two-particle predictions $\langle x^1(t)^2\rangle$ in agreement with the preceding perturbation analysis. There is good quantitative agreement between the two-particle prediction and the full numerical results in the early-time behaviour. We note, in particular, that the rate of long-term growth decreases rapidly as Γ increases, in agreement with the predicted lack of long-time growth in figure 6. We note also that the implication that D_{xx} is $o(\Gamma^{-2})$ in (5.12) is consistent with the numerical results in figure 3 showing that D_{xx} has a scaling somewhere between Γ^{-3} and Γ^{-4} as Γ is increased.

Figure 8(a) shows the scaled mean-square displacements $\langle\Delta y^2\rangle/\Gamma^{-2}$ from the full calculations with $L=15$ and various values of Γ. Again, these scaled displacements collapse onto the leading-order two-particle displacements $\langle y^1(t)^2\rangle$ as Γ is increased, in accordance with the perturbation analysis. Figure 8(b) shows that there is a corresponding convergence of the scaled diffusion coefficients $D_{yy}/(L\Gamma^{-2})$ onto the two-particle prediction (5.12) that $D_{yy}/(L\Gamma^{-2})\sim 9.4\times10^{-4}$ as Γ is increased. Figure 8(b) also shows that the scaled diffusion coefficients, for all the values of L and Γ considered, collapse onto the same curve when plotted against the inverse

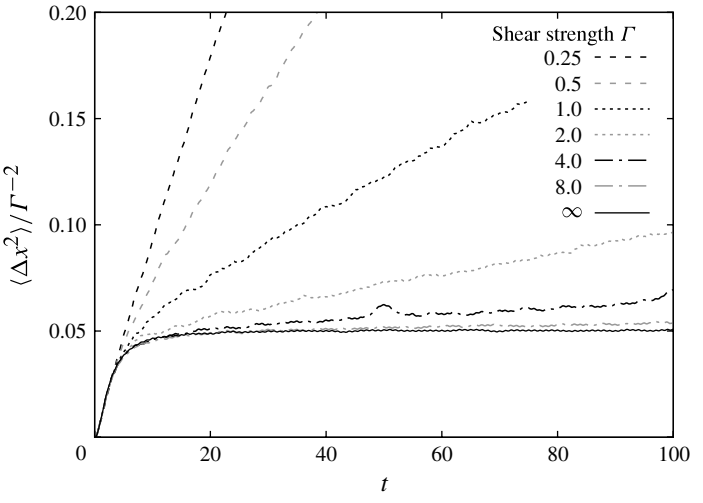

FIGURE 7. Evolution of $\langle \Delta x^2 \rangle / \Gamma^{-2}$ for $L = 15$ and varying values of the shear strength Γ. As Γ is increased, the curves collapse onto the the two-particle prediction $\langle x^1(t)^2 \rangle$ (marked as $\Gamma = \infty$), which asymptotes to a constant value.

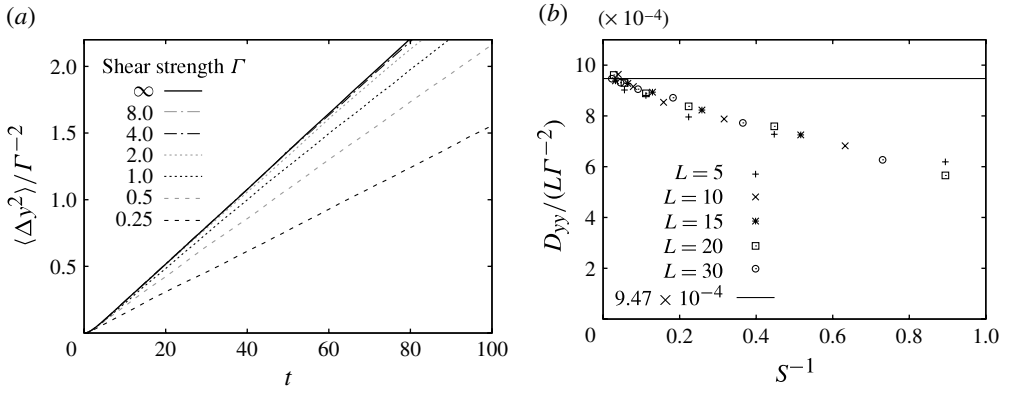

FIGURE 8. (*a*) Evolution of $\langle \Delta y^2(t) \rangle / \Gamma^{-2}$ for $L = 15$ and varying shear strength Γ. As Γ is increased, the curves collapse onto the two-particle prediction $\langle y^1(t)^2 \rangle$ (marked as $\Gamma = \infty$). (*b*) The corresponding hydrodynamic diffusion coefficients D_{yy} calculated from the period $20 \leqslant t \leqslant 100$. The diffusion coefficients are scaled by the predicted $L\Gamma^{-2}$ scaling, and the predicted value from two-particle interactions, 9.47×10^{-4}, is marked by a horizontal line. The data are plotted against the inverse of the system-scale ratio $S = L^{1/2}\Gamma$ of the shear velocity to hydrodynamic velocity fluctuations.

of the system-scale ratio $S = L^{1/2}\Gamma$ of the shear velocity to hydrodynamic velocity fluctuations, with convergence to (5.12) as $S \to \infty$.

Overall, we conclude that the predictions that emerge from two-particle interactions in the perturbation analysis are in good agreement with the numerical results for sufficiently large values of S.

5.3. *Behaviour of a two-particle interaction*

The $O(\Gamma^{-1})$ leading-order horizontal displacements (5.6) are a sum of $N-1$ independent two-particle interactions. To explain why these two-particle interactions do not give rise to diffusive growth in the x-direction (figure 6), we analyse the properties of a single two-particle interaction by considering a system with only two particles ($N=2$). Such a system has no three-particle interactions, so the perturbation analysis terminates at $O(\Gamma^{-1})$.

The particle velocities (subtracting, for simplicity, the velocity induced on each particle by its own images) are given by

$$\frac{\mathrm{d}\boldsymbol{x}_i}{\mathrm{d}t} = (\boldsymbol{x}_i \cdot \boldsymbol{e}_x)\boldsymbol{e}_z + \Gamma^{-1}\,\boldsymbol{u}^p(\boldsymbol{x}_{12}(t), t) \tag{5.13}$$

for $i=1,2$. Each particle induces the same velocity $\Gamma^{-1}\,\boldsymbol{u}^p$ on the other, the value of which depends on the separation $\boldsymbol{x}_{12}=\boldsymbol{x}_1-\boldsymbol{x}_2$ of the particles. Consequently, the separation between the particles only changes due to the background shear, and is given by

$$\boldsymbol{x}_{12}(t) = \boldsymbol{x}_{12}(0) + t(\boldsymbol{x}_{12}(0)\cdot\boldsymbol{e}_x)\boldsymbol{e}_z. \tag{5.14}$$

The periodic nature of the system complicates the behaviour of this 'two-particle' interaction since the interaction includes that with all the images of the other particle. To simplify the discussion, we temporarily switch to considering an unbounded domain. In this case, the separation of the particle pair evolves as before, but the periodic Stokeslet velocity $\boldsymbol{u}^p(\boldsymbol{x},t)$ in (5.13) is replaced by the unbounded Stokeslet velocity

$$\boldsymbol{u}^u(\boldsymbol{x}) = \frac{1}{8\pi}\boldsymbol{e}_z \cdot \left(\frac{\boldsymbol{I}}{|\boldsymbol{x}|} + \frac{\boldsymbol{x}\boldsymbol{x}}{|\boldsymbol{x}|^3}\right). \tag{5.15}$$

The horizontal velocity components of (5.15) are

$$u^u(\boldsymbol{x}) = \frac{1}{8\pi}\frac{xz}{|\boldsymbol{x}|^3}, \quad v^u(\boldsymbol{x}) = \frac{1}{8\pi}\frac{yz}{|\boldsymbol{x}|^3}, \tag{5.16}$$

from which the horizontal displacements can be found analytically as

$$\Delta x_i(t) = \frac{1}{8\pi\Gamma}\left((x_0^2+y_0^2+z_0^2)^{-1/2} - (x_0^2+y_0^2+(z_0+x_0t)^2)^{-1/2}\right), \tag{5.17a}$$

and

$$\Delta y_i(t) = \frac{1}{8\pi\Gamma}\frac{y_0}{x_0}\left((x_0^2+y_0^2+z_0^2)^{-1/2} - (x_0^2+y_0^2+(z_0+x_0t)^2)^{-1/2}\right), \tag{5.17b}$$

where $\boldsymbol{x}_0=(x_0,y_0,z_0)$ is the separation of the particles at $t=0$.

A typical unbounded two-particle interaction is shown in figure 9. There are two important features of such interactions. Firstly, there is no net horizontal displacement, i.e. $\Delta x_i(-\infty)=\Delta x_i(\infty)$ and $\Delta y_i(-\infty)=\Delta y_i(\infty)$. This is a consequence of the reversibility of Stokes flow, which implies that the flow after $t=-z_0/x_0$ when the particles have the same height can be obtained from that for $t<-z_0/x_0$ by reflecting in the horizontal plane through the particles and reversing time.

Secondly, the typical magnitudes of the horizontal displacements relative to the positions at $t=\pm\infty$ have different forms in the x- and y-directions. For example, the

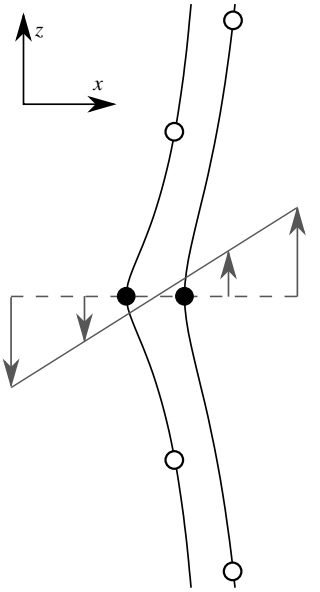

FIGURE 9. A pair of particles rises relative to the shear flow and drifts sideways due to the hydrodynamic interaction between the particles. The separation of the particles changes due to the shear flow so that the interaction has finite duration. Circles show the particle positions at three successive times. The horizontal displacement of the particles is symmetric about the point when the particles are at the same height (filled circles) implying that there is no net horizontal displacement from the full interaction.

maximum displacements are given by (5.17) as

$$\Delta x_M = \frac{1}{8\pi\Gamma}\frac{1}{r_0} \quad \text{and} \quad \Delta y_M = \frac{1}{8\pi\Gamma}\frac{y_0}{x_0}\frac{1}{r_0}, \tag{5.18}$$

where $r_0 \equiv (x_0^2 + y_0^2)^{1/2}$ is the horizontal separation between the particles. We can understand these magnitudes from a simple scaling argument. The dominant interaction between the two particles occurs while their vertical separation is comparable to (or less than) their horizontal separation, since the horizontal velocities decrease rapidly with vertical separation. The vertical separation varies at a rate x_0 due to the background shear flow, and so the duration of the dominant interaction is order r_0/x_0. During this time, the typical horizontal velocity of the pair, $1/(\Gamma r_0)$, leads to a typical horizontal displacement $1/(\Gamma x_0)$ in the direction (x_0, y_0). The scalings of (5.18) are recovered by resolving this displacement in the x- and y-directions.

Returning to a periodic system with many particles: the $O(\Gamma^{-1})$ leading-order horizontal displacements are given by (5.6) as the sum of two-particle interactions with each of the $N-1$ other particles and their images; furthermore, the periodic system of N particles and their images can be viewed as an unbounded system containing infinitely many particles, which happen to be placed in a periodic manner. Thus, the leading-order displacements can be viewed as the sum of many unbounded two-particle interactions, each of which causes no net displacement.

This lack of a net horizontal displacement plays a vital role in determining the diffusive behaviour of a vertically sheared system. It provides an explanation for why two-particle interactions do not give rise to diffusive growth in the x-direction

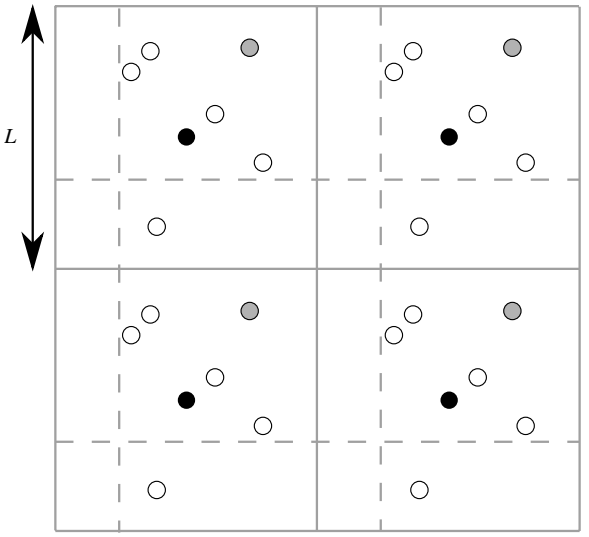

FIGURE 10. The quasi-periodic simplification of hydrodynamic interactions (shown in two dimensions for clarity). Hydrodynamic interactions with a given particle are limited to those arising from a cube of side L centred on that particle. For example, the velocity of each black particle is calculated using only the hydrodynamic contributions from the six other particles in the solid box centred on that particle; the velocity of each grey particle is calculated using only the hydrodynamic contributions from the six other particles in the dashed box centred on that particle.

(figure 6) and hence why $D_{xx} = o(\Gamma^{-2})$. It also raises a surprising point that requires further explanation: displacements due to two-particle interactions cause no net displacement in both the x- and y-directions, yet two-particle interactions do give rise to a diffusion-like growth of mean-square displacements in the y-direction (figure 6).

5.4. *Analysis of the mean-square displacements due to two-particle interactions: a quasi-periodic model*

In this section we show how the combination of individual two-particle interactions, which cause no net horizontal displacement, and the ensemble average over all such interactions, which is required to calculate mean-square displacements, leads to an asymptotically constant mean-square displacement in the x-direction, but to a linearly growing mean-square displacement in the y-direction (figure 6).

Analysis of the fully periodic system is mathematically complicated, and we defer it to appendix A. To develop an understanding of the physical origins of the difference in behaviour between the x- and y-directions, we work with a simpler quasi-periodic model that still captures the essential physical mechanisms.

In the fully periodic system, the hydrodynamic velocity of each particle is given by the sum of Stokeslet contributions from all the other particles and all their periodic images. We define a quasi-periodic model as follows: we consider the same collection of particles and images, but we approximate the hydrodynamic velocity of each particle by the sum only of the Stokeslet contributions from those particles and images that happen to lie within a cube of side L centred on that particle (see figure 10). Contributions from particles and images outside this cube are omitted. This

model treats all particles equally, since each particle is at the centre of its own cube. A similar trick has been successfully used to model the dynamics of other periodic systems numerically (Kerr, Lister & Mériaux 2008; Lister *et al.* 2011; Crosby & Lister 2012).

In the quasi-periodic model, the horizontal displacement due to a single two-particle interaction, $\Gamma^{-1}\boldsymbol{X}_L^H(\boldsymbol{x},t)$, has a simple analytic form, which is closely related to that for an unbounded domain (5.17). Only one of the periodic images of the second particle is in the cube of side L centred on the first particle at any given time. The displacement of the first particle, due to the image of the second particle that is currently in the cube, is exactly that due to a particle in an unbounded domain (5.17). This image particle is advected by the background shear until it leaves either the top or the bottom of the cube, at which point it no longer induces a velocity on the first particle. However, at the same time, another one of the second particle's images enters the cube at the same horizontal position on the opposite side. The process repeats, leading to a sequence of displacements to the first particle, each of which corresponds to the section of the displacement due to a second particle in an unbounded domain for which the vertical separation of the second particle relative to the first particle is in the range $-L/2 < z \leqslant L/2$, and each of which causes no net horizontal displacement. Consequently, the horizontal displacements of the first particle due to a second particle at initial separation $\boldsymbol{x}$ and its images can be written as

$$\Gamma^{-1}X_L(\boldsymbol{x},t) = \frac{1}{8\pi\Gamma}\left\{\left(x^2+y^2+z^2\right)^{-1/2} - \left(x^2+y^2+L^2\,\mathrm{frac}\left(\frac{z+xt}{L}\right)^2\right)^{-1/2}\right\} \tag{5.19a}$$

and

$$\Gamma^{-1}Y_L(\boldsymbol{x},t) = \frac{1}{8\pi\Gamma}\frac{y}{x}\left\{\left(x^2+y^2+z^2\right)^{-1/2} - \left(x^2+y^2+L^2\,\mathrm{frac}\left(\frac{z+xt}{L}\right)^2\right)^{-1/2}\right\} \tag{5.19b}$$

(cf. (5.17)), where $\mathrm{frac}(s)$ is defined to be the fractional part of s in the range $-1/2 < s \leqslant 1/2$. The effect of the function $\mathrm{frac}(s)$ is to pick out the appropriate section of the unbounded two-particle interaction for which the second particle is at a vertical separation in the range $-L/2 < z \leqslant L/2$.

We now consider the implications of (5.19) for the mean-square displacements. The leading-order approximation to the mean-square displacement in the x-direction (scaled by Γ^{-2}) follows from (5.11) and (5.19*a*):

$$\langle x^1(t)^2\rangle = \frac{L}{(8\pi)^2}\int_{V(1)}\left\{\left(x^2+y^2+z^2\right)^{-1/2} - \left(x^2+y^2+\mathrm{frac}(z+xt)^2\right)^{-1/2}\right\}^2 \mathrm{d}^3\boldsymbol{x}. \tag{5.20}$$

Expanding the square in the integrand, and omitting the negative cross-term, we find that $\langle x^1(t)^2\rangle$ must be bounded since the two positive terms give

$$\begin{aligned}\langle x^1(t)^2\rangle &\leqslant \frac{2L}{(8\pi)^2}\int_{V(1)}\left(x^2+y^2+z^2\right)^{-1}\mathrm{d}^3\boldsymbol{x}\\ &= 2.43\times10^{-2}L.\end{aligned} \tag{5.21}$$

This bound on $\langle x^1(t)^2\rangle$ is consistent with the asymptotic convergence to a constant value in figure 6. The asymptotic value can be predicted by calculating the time-

averaged mean-square displacement from a time-integration of (5.20). A detailed calculation shows that $\overline{\langle x^1(t)^2\rangle} = 3.80 \times 10^{-3}L$. This value differs slightly from that in figure 6 owing to the use of quasi-periodicity, rather than true periodicity, in this section.

Similarly, in the y-direction, the leading-order approximation to the mean-square displacement follows from (5.11) and (5.19*b*):

$$\langle y^1(t)^2\rangle = \frac{L}{(8\pi)^2}\int_{V(1)} \frac{y^2}{x^2}\left\{(x^2+y^2+z^2)^{-1/2} - (x^2+y^2+\mathrm{frac}(z+xt)^2)^{-1/2}\right\}^2 \mathrm{d}^3\boldsymbol{x}. \quad (5.22)$$

Attempting to apply the same technique as for (5.21), we find that

$$\langle y^1(t)^2\rangle \leqslant \frac{2L}{(8\pi)^2}\int_{V(1)} \frac{y^2}{x^2}(x^2+y^2+z^2)^{-1}\,\mathrm{d}^3\boldsymbol{x}. \quad (5.23)$$

However, this integral is infinite owing to a divergent contribution near $x = 0$ from the factor (y^2/x^2). This lack of success in bounding $\langle y^1(t)^2\rangle$ should, of course, be expected given the unbounded growth observed in figure 6.

The extra factor y/x in the y-displacements (compare (5.19*b*) and (5.19*a*)) is responsible for the different behaviours of $\langle x^1(t)^2\rangle$ and $\langle y^1(t)^2\rangle$, and leads to the dominance in (5.22) of two-particle interactions that satisfy $x^2 \ll y^2$. In physical terms, these are the interactions in which both particles are in, or close to, the same plane of the shear flow. Such nearly coplanar particles differ only slightly in shear velocity and, consequently, have a long interaction time (see figure 11). We refer to these particles as weakly sheared. The long interaction time of weakly sheared particles leads to much larger horizontal displacements of these particles than those of other particles with the same horizontal separation and, since the displacements of weakly sheared particles are predominantly in the y-direction, they dominate (5.22). Conversely, the weakly sheared interactions do not dominate the mean-square displacement in the x-direction (5.20) because only a small proportion of their large horizontal displacement is in the x-direction.

We determine the long-time behaviour of $\langle y^1(t)^2\rangle$ in (5.22) by focusing on the contribution from the weakly sheared interactions, which dominate the integral at large times. To do this, we make the change of spatial variable $s = xt$:

$$\langle y^1(t)^2\rangle = \frac{Lt}{(8\pi)^2}\int_{-1/2}^{1/2}\int_{-1/2}^{1/2}\int_{-t/2}^{t/2}\frac{y^2}{s^2}\left(\left\{\left(\frac{s}{t}\right)^2+y^2+z^2\right\}^{-1/2} - \left\{\left(\frac{s}{t}\right)^2+y^2+\mathrm{frac}(z+s)^2\right\}^{-1/2}\right)^2 \mathrm{d}s\,\mathrm{d}y\,\mathrm{d}z. \quad (5.24)$$

If s is $O(1)$ as $t \to \infty$ then the integrand in (5.24) is also $O(1)$, but when s is $O(t)$, the integrand is only $O(t^{-2})$ due to the factor of s^{-2}. Overall, the integral consists of an $O(1)$ contribution from $O(1)$ values of s and an $O(t^{-1})$ contribution from $O(t)$ values of s. Thus, for $t \gg 1$, the dominant contribution to the integral comes from values of s with $s \ll t$. Consequently, we can obtain the leading-order behaviour of (5.24) as $t \to \infty$ by replacing the limits of the inner integral over s with $\pm\infty$ and neglecting

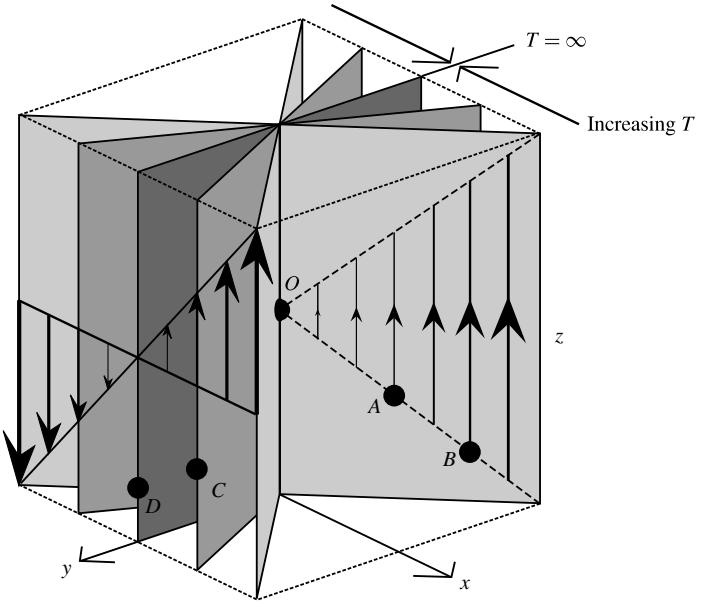

FIGURE 11. The interaction time between a given particle O and a second particle (A, B, C or D) depends on the orientation of the vertical plane containing the two particles. Each of particles A and B, and any other particles in the lightly shaded plane, takes the same time to be advected past O through a vertical distance that is comparable to its horizontal separation from O (e.g. through the distance between the dashed lines). Particle C is more weakly sheared and takes longer to advect past O than A or B. Particle D lies in the same shear-plane as O and can only advect past O if third-particle interactions nudge O or D into a neighbouring shear-plane. The duration T of purely two-particle interactions is proportional to $(x^2 + y^2)^{1/2}/x$ and increases towards infinity the closer the orientation of the plane containing the particles is to a shear-plane.

the $(s/t)^2$ terms in the integrand. This gives the leading-order behaviour for large t as

$$\langle y^1(t)^2 \rangle \sim \frac{Lt}{(8\pi)^2} \int_{-1/2}^{1/2} \int_{-1/2}^{1/2} \int_{-\infty}^{\infty} \frac{y^2}{s^2} \left(\left(y^2 + z^2\right)^{-1/2} - \left(y^2 + \mathrm{frac}(z+s)^2\right)^{-1/2} \right)^2 \mathrm{d}s\,\mathrm{d}y\,\mathrm{d}z$$
$$= 2.6 \times 10^{-3} Lt. \tag{5.25}$$

The linear growth of $\langle y^1(t)^2 \rangle$ with t for $t \gg 1$ is not due to the usual mechanism in which a particle undergoes a random walk consisting of a series of many small random displacements due to interactions with a succession of other particles. Indeed, it cannot be since each image that passes through the cube surrounding the particle causes no net displacement. Instead, we can understand the physical mechanism by noting that the integral in (5.24) is dominated by $O(1)$ values of y and z, and, for $t \gg 1$, by $O(1)$ values of s, which correspond to $O(1/t)$ values of x. These values correspond to interactions with particles whose separation in the y- and z-directions is comparable to the system size (remembering that we have scaled out the length L) but which, crucially, have a small separation in the x-direction and are thus weakly sheared by the background flow. We deduce that the linear growth of the mean-square displacements is a result of $O(t^2)$ ballistic contributions to the square displacements from those particles that lie within the $O(1/t)$ wide interval in x in which the particles

are sufficiently weakly sheared that the interactions are lasting longer than t. Since these particles have only undergone a fraction of their interaction, the lack of a net displacement from the full interaction is not yet a limiting factor.

Very similar physical and mathematical arguments apply to the fully periodic system (see appendix A) since the periodic Stokeslet, despite its complexity, has similar properties to the simple Stokeslet of the quasi-periodic model. Numerical evaluation of the integrals analogous to (5.20) and (5.25) predicts the following values for the time-averaged x-displacements and asymptotic linear growth of the y-displacements:

$$\overline{\langle x^1(t)^2\rangle} = 3.34 \times 10^{-3} L, \quad \langle y^1(t)^2\rangle \sim 1.89 \times 10^{-3} Lt. \tag{5.26}$$

From (2.10) and (5.9), the resulting diffusion coefficient from two-particle interactions in the y-direction is

$$D_{yy} \sim 9.47 \times 10^{-4} L\Gamma^{-2}. \tag{5.27}$$

These asymptotic values are slightly smaller than the quasi-periodic results, and are in very good agreement with the values found earlier by numerical integration of the time-dependent problem (see (5.11) and figure 6).

It should be noted that the mechanisms described in this section do not fundamentally depend upon the vertical periodicity of the system: similar results would hold for a vertically infinite system.

6. Multi-particle interactions

6.1. *Behaviour of D_{xx} for $\Gamma \gg 1$*

As we have shown in the previous section, two-particle interactions alone are not sufficient to lead to diffusive growth in the x-direction, and the inclusion of at least three-particle interactions is necessary. The net displacement due to a second particle is no longer zero when the effect of a third particle, which perturbs the separation between the first two particles, is taken into account. Here we use a scaling argument to determine the contribution to hydrodynamic diffusion from these three-particle interactions. This argument highlights the important physical processes, and is able to explain the earlier numerical observations that D_{xx} has a scaling somewhere between Γ^{-3} and Γ^{-4} as Γ increased (figure 3*a*) and a sub-linear scaling with L (figure 4*a*).

The key idea behind the scaling argument is the same as that behind the earlier perturbation analysis in § 5.1: for strongly sheared systems ($\Gamma \gg 1$) the vast majority of interactions between particles are dominated by the shear flow, with hydrodynamic velocities providing only a small perturbation. The hydrodynamic velocity fluctuations are limited by the periodicity of the system to scales smaller than the system size L, which thus acts as a large-scale cutoff for hydrodynamic interactions in the scaling argument. Interactions with a given particle on scales smaller than L are dominated by the nearest of the particle's periodic images, and can simply be treated as interactions with only the nearest image in an unbounded domain.

Consider two isolated particles at a separation of $\boldsymbol{x}$. The bulk of the interaction of these particles occurs during the period in which their vertical separation is comparable to (or less than) their horizontal separation, $z^2 \sim x^2 + y^2$. Outside this period, when $z^2 \gg x^2 + y^2$, the horizontal component of the velocity that each particle induces on the other is very much smaller by a factor of $O[(x^2 + y^2)/z^2]$, and the corresponding contribution to the horizontal displacement is negligible. Unless the particles have exactly the same x-coordinate, the shear flow causes the vertical

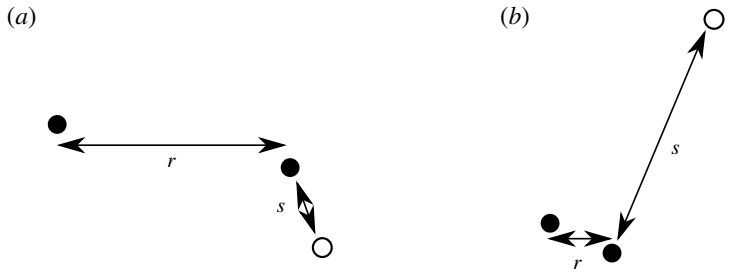

FIGURE 12. The strain rate due to a third particle (open circle) at a separation s from a particle pair of separation r (closed circles) depends on their relative separations: (*a*) if $s \lesssim r$, then the third particle induces a much larger velocity on one particle than the other; (*b*) if $s \gtrsim r$, then both particles in the pair are at a similar position relative to the third particle and experience its straining field at that point.

separation of the particles to change at a rate x, so that the typical interaction time is $O(r/x)$, where $r \equiv (x^2 + y^2)^{1/2}$ is the horizontal separation between the two particles. During their interaction, the two particles undergo a displacement in the x-direction of $O(\Gamma^{-1}r^{-1})$ (cf. (5.18)), but this displacement is later reversed to leave no net displacement from the full interaction (figure 9). However, if flow due to other particles changes the separation between the two particles during their interaction, then their horizontal displacements will not be exactly reversed and there will be a net displacement. By estimating the magnitude of the unreversed portion of the horizontal displacement, first due to the effect of a single third particle and then due to the cumulative effect of many third particles, we will obtain an estimate of the mean-square displacement and thence of D_{xx}.

Before doing so, we note that there is a narrow range of horizontal orientations of the two particles for which the typical interaction time $O(r/x)$ is large compared to the $O(1)$ shear time scale. These are the so-called 'weakly sheared' particles with $x \ll r$. Since pairs of particles involved in weakly sheared interactions induce only a weak $O(x/r^2)$ velocity in the x-direction on each other, and since only a small proportion of the particle pairs are weakly sheared, we can assume that the dominant contribution to displacements in the x-direction and hence to D_{xx} does not arise from these weak interactions. The majority of particle pairs (those with $x \sim r$) are not weakly sheared and interact on the $O(1)$ shear time scale, and we will focus on these interactions below.

Consider the effect of a third particle on the interaction of two particles. The strain rate due to this third particle causes the separation of the first two particles to vary, leading to an unreversed portion of the displacement. The magnitude of this strain rate depends on the separation s of the third particle relative to the nearest of the other two particles. There are two cases to consider depending on the value of s (figure 12): if $s \ll r$, then the third particle induces an $O(\Gamma^{-1}s^{-1})$ velocity on one of the first two particles and a much smaller velocity on the other, giving an average strain rate over the distance between the particles of $O(\Gamma^{-1}r^{-1}s^{-1})$; if $s \gg r$, then the first two particles are at approximately the same position relative to the third particle, and experience the $O(\Gamma^{-1}s^{-2})$ straining field at that point. (The two cases match smoothly for $s \sim r$.) The separation between the first two particles is changed by the accumulated strain, which is given by multiplying the strain rate by the $O(1)$

interaction time to obtain a strain of magnitude

$$\epsilon(r,s) \sim \begin{cases} \Gamma^{-1} r^{-1} s^{-1} & s \lesssim r, \\ \Gamma^{-1} s^{-2} & s \gtrsim r. \end{cases} \tag{6.1}$$

In the strong shear limit $\Gamma \gg 1$, most hydrodynamic interactions have $r, s \gtrsim \Gamma^{-1/2}$ and hence the corresponding strain satisfies $\epsilon(r,s) \ll 1$. For these interactions, the unreversed proportion of the $O(\Gamma^{-1} r^{-1})$ displacement should depend linearly upon $\epsilon(r,s)$. Thus the magnitude of the unreversed displacement, $\Delta x(r,s)$, for a single three-particle interaction scales as

$$\Delta x(r,s) \sim \frac{\epsilon(r,s)}{\Gamma r} \sim \begin{cases} \Gamma^{-2} r^{-2} s^{-1} & s \lesssim r, \\ \Gamma^{-2} r^{-1} s^{-2} & s \gtrsim r. \end{cases} \tag{6.2}$$

The separation of the first two particles is perturbed by many such third particles. Since the unreversed displacement due to each of the individual third particles is equally likely to be in the positive or the negative x-direction, there is significant cancellation in the magnitude of the overall unreversed displacement. To account for this cancellation, we consider the variance of the displacements. The variance of a sum of independent displacements with zero mean is given by the sum of the individual variances. The variance of the displacement from a single third particle scales as $\Delta x(r,s)^2$, so the variance of the overall displacement from all third particles, $\Delta X(r)^2$, scales as

$$\Delta X(r)^2 \sim \int_0^L \Delta x(r,s)^2 p(s)\,\mathrm{d}s, \tag{6.3}$$

where $p(s)$ is the probability density of finding a third particle at a separation s. As noted in § 2, the probability distribution of the particles is uniform at $t = 0$, and remains so, and so $p(s) \sim s^2$ for both $s \lesssim r$ and $s \gtrsim r$.

Combining (6.2) and (6.3) gives

$$\begin{aligned} \Delta X(r)^2 &\sim \Gamma^{-4} \int_0^r \left(r^{-2} s^{-1}\right)^2 s^2 \,\mathrm{d}s + \Gamma^{-4} \int_r^L \left(r^{-1} s^{-2}\right)^2 s^2 \,\mathrm{d}s \\ &\sim \frac{1}{\Gamma^4 r^3}. \end{aligned} \tag{6.4}$$

The dominant contribution to the integrals comes from $s \sim r$, which implies physically that the dominant contribution to the unreversed displacement of a pair of particles comes from interactions with a third particle at a similar separation to that of the pair.

Equation (6.4) applies for $r \gtrsim \Gamma^{-1/2}$, since it was based on the assumption that $\epsilon(r,s) \ll 1$. A few hydrodynamic interactions have $r \lesssim \Gamma^{-1/2}$, and for these interactions, the $O(r)$ shear flow is no longer strong compared to the $O(\Gamma^{-1} r^{-1})$ hydrodynamic velocities. Instead, a single third particle at a similar separation to the first two generates an $O(1)$ strain leading to a completely unreversed displacement. Detailed consideration of various types of three-particle interaction shows that the magnitude of the unreversed displacement is reduced from (6.4) and instead given by $\Delta X(r)^2 \sim \Gamma^{-3} r^{-1}$ for $r \lesssim \Gamma^{-1/2}$.

Interactions between two particles at a horizontal separation r occur with some frequency density $f(r)$. The scaling for $f(r)$ can be found from considering a horizontal slice through the system: the number density of particles at separation r in the slice scales as r, and the velocity of particles relative to the test particle

also scales as r; hence $f(r) \sim r^2$. Each interaction between two particles leads to a net displacement of magnitude $\Delta X(r)$ in the x-direction, due to the three-particle effects that we have just analysed. As a result of many such interactions, the particle displacement undergoes a horizontal motion like a random walk. The diffusion coefficient can be calculated from the mean-square displacements $\Delta X(r)^2$ weighted by the frequency density $f(r)$:

$$\begin{aligned} D_{xx} &\sim \int_0^L \Delta X(r)^2 f(r)\,\mathrm{d}r \\ &\sim \int_0^{\Gamma^{-1/2}} \left(\frac{1}{\Gamma^3 r}\right) r^2\,\mathrm{d}r + \int_{\Gamma^{-1/2}}^{L} \left(\frac{1}{\Gamma^4 r^3}\right) r^2\,\mathrm{d}r \\ &\sim \Gamma^{-4}\ln(L\Gamma^{1/2}) + O(\Gamma^{-4}). \end{aligned} \tag{6.5}$$

The physical interpretation of the logarithmic term is that D_{xx} is not dominated by interactions at a particular horizontal separation r, but rather by contributions from the whole range of separations between the system size L and the scale $\Gamma^{-1/2}$ on which hydrodynamic interactions start to dominate shear.

The predicted scaling, $D_{xx} \sim \Gamma^{-4}\ln(L\Gamma^{1/2})$, is consistent with our earlier numerical observations that D_{xx} had a scaling somewhere between Γ^{-3} and Γ^{-4} and a sub-linear scaling with L. Including the $O(1)$ coefficients of proportionality in the scaling arguments, we predict that

$$\begin{aligned} D_{xx} &\sim \alpha\Gamma^{-4}\ln(\tilde{\beta}L\Gamma^{1/2}) \\ &\sim \alpha\Gamma^{-4}\ln(L\Gamma^{1/2}) + \beta\Gamma^{-4}. \end{aligned} \tag{6.6}$$

The form of (6.6) suggests looking at a compensated plot of $D_{xx}/(\Gamma^{-4}\ln(L\Gamma^{1/2}))$ against $1/\ln(L\Gamma^{1/2})$, which should be a straight line with intercept α and gradient β. From a linear fit to the data in figure 13, we estimate that $\alpha \approx 4.2 \times 10^{-4}$ and $\beta \approx -3.6 \times 10^{-4}$ (implying that $\tilde{\beta} = 0.42$). Due to the slow growth of the logarithmic term, the order Γ^{-4} correction term is still numerically significant for even the largest values of the shear strength Γ that we were able to simulate numerically.

6.2. *Impact of multi-particle interactions on the very-long-time behaviour of D_{yy}*

When simulations are evolved for a fixed shear time, there is a very good agreement between the observed linear growth of the mean-square displacement in the y-direction for $t \gg 1$ and the diffusivity predicted by two-particle interactions, $D_{yy} \sim 9.47 \times 10^{-4} L\Gamma^{-2}$ (5.12), with convergence as $S \to \infty$ (figure 8*b*), where $S = L^{1/2}\Gamma$ is the ratio of the shear velocity to hydrodynamic velocity fluctuations on the scale of the system. However, in § 5.1 we noted that the approximation of the mean-square displacement by the leading-order two-particle approximation might not be valid for all time. In this section we argue that, indeed, the effects of multi-particle interactions can no longer be neglected at very long times, leading to another regime with slightly smaller diffusion coefficient. The need for a new regime can be understood by the following simple argument.

The linear growth of the mean-square displacement is due to ballistic displacements from two-particle interactions within a small region of weakly sheared particles (§ 5.4). The width of this region in the x-direction is $O(L/t)$ and decreases with time. Consequently, the typical shear velocity between two particles in this region, which is proportional to their separation in the x-direction, also decreases with time. Underlying the perturbation analysis in § 5 was the assumption that the shear velocity between

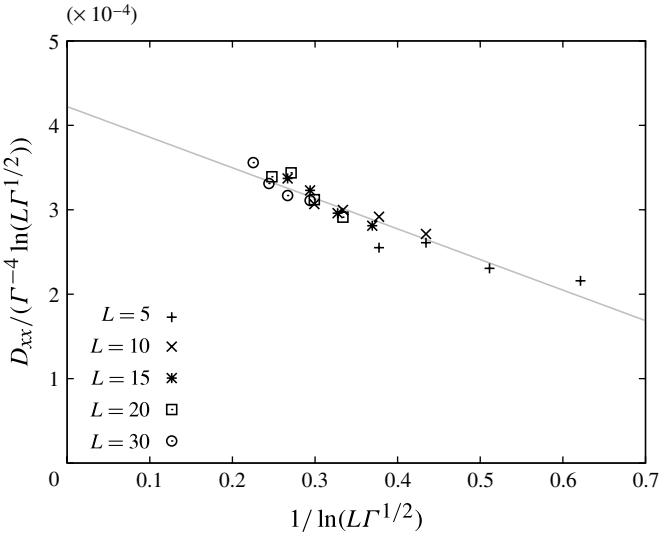

FIGURE 13. Diffusion coefficients D_{xx} for $\Gamma \geqslant 1$ scaled by $\Gamma^{-4}\ln(L\Gamma^{1/2})$ and plotted against $1/\ln(L\Gamma^{1/2})$. Also shown is a linear fit to the data $4.22 \times 10^{-4} - 3.62 \times 10^{-4}x$ (grey line); such linear behaviour is consistent with the prediction (6.6) from scaling arguments. The collapse of scaled values of D_{xx} exhibited here should be contrasted with figures 3(*a*) and 4(*a*) in which the corresponding unscaled values of D_{xx} can be seen to vary by several orders of magnitude with Γ and by an order of magnitude with L.

two particles is sufficiently strong compared to hydrodynamic velocity fluctuations that the path of one particle relative to another was a vertical straight line at leading order. Eventually, the $O(L/t)$ width of the ballistic region will become sufficiently narrow, and the particles within it sufficiently weakly sheared, that this assumption no longer holds. On this time scale, the two-particle approximation must break down, and we expect a transition to a new regime in which multi-particle interactions are important.

To test this idea, the evolution of $\langle \Delta y(t)^2 \rangle$ was calculated for an extended period of time and is shown in figure 14(*a*) for the case $L = 15$ and $\Gamma = 4$. Initially, for approximately eighty shear times ($t \lesssim 80$), there is good agreement with the rate of linear growth predicted by the two-particle approximation. Then, on a similar time scale, there is a subtle transition to another regime, which again exhibits linear growth but with a slightly smaller gradient. Figure 14(*b*) shows the gradient of the (smoothed) mean-square displacement. The transition is evident despite the statistical noise. This transition is consistent with our expectation that the two-particle approximation will eventually break down and give way to a regime in which multi-particle interactions are important. We refer to this later regime as the very-long-time regime.

The transition shown in figure 14 for the case $L = 15$ and $\Gamma = 4$ is quite subtle because there is a decrease in gradient of only 14 % over a period of several hundred shear times. Such behaviour seems to be generic for $S \gg 1$. Diffusion coefficients calculated from a linear fit to the period $20S \leqslant t \leqslant 40S$ for a range of parameters (all with $S \gg 1$) are shown in figure 15 alongside the values that were previously calculated from a linear fit to the earlier period $20 \leqslant t \leqslant 100$ (figure 8*b*). In all cases, the diffusion coefficients calculated from the later period are reduced from their earlier values, but only slightly; the largest decrease is 26 % for $L = 5$ and $\Gamma = 8$.

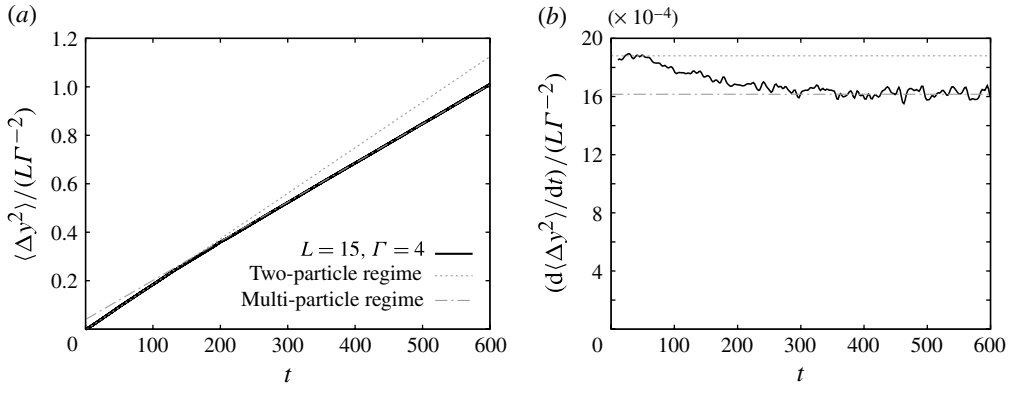

FIGURE 14. (*a*) Very-long-time evolution of the (scaled) mean-square displacement in the y-direction for $L = 15$ and $\Gamma = 4$ averaged over 600 simulations containing a total of 2×10^6 particles (black line). The statistical uncertainty is comparable to the width of the line. Also shown are the asymptotic linear growth with gradient 1.89×10^{-3} predicted by the two-particle approximation (5.26) (dashed grey line), and a linear fit to the period $400 \leqslant t \leqslant 800$ which has a smaller gradient 1.62×10^{-3} (dot-dashed grey line). (*b*) The local gradient of the (scaled) mean-square displacement shown in (*a*), calculated after smoothing the data over a time-window of length 10 and excluding three outlying simulations in order to reduce statistical noise. Initially, for $t \lesssim 80$, the gradient matches the two-particle approximation. Then, on a similar time scale, the gradient falls to a slightly smaller value, which we suggest corresponds to a transition into a new very-long-time regime.

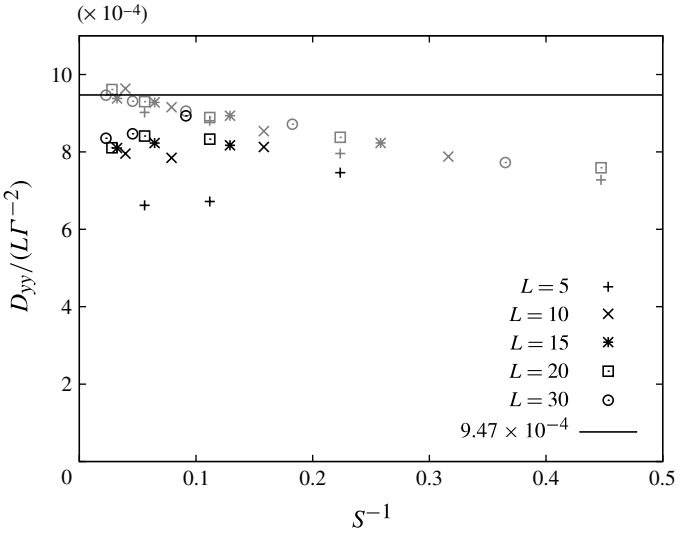

FIGURE 15. Diffusion coefficients calculated from the period $20 \leqslant t \leqslant 100$ (grey symbols), which converge to the two-particle approximation as $S = L^{1/2}\Gamma \to \infty$ (as shown in figure 8*b*), and coefficients calculated from a later period $20S \leqslant t \leqslant 40S$ (black symbols), which have slightly smaller values. Each diffusion coefficient is calculated from an ensemble of simulations containing at least 10^5 particles.

We now present two scaling arguments: one demonstrating that the very-long-time diffusivities should scale as $D_{yy} \sim L\Gamma^{-2}$ independently of the time at which the two-particle approximation breaks down, and another suggesting that the breakdown occurs when $t \sim S$.

When the two-particle approximation breaks down, we expect the dominant contribution to the mean-square displacement in the y-direction to arise from those interactions for which the horizontal displacement is not reversed: these are the interactions that are sufficiently weakly sheared, due to a small separation in the x-direction, that the path of one particle relative to the other is not well approximated by a vertical straight line. Suppose that Λ, to be determined, is the width of the planar region of small separations in the x-direction that lead to unreversed displacements. The contribution to the displacement of a given particle in the y-direction from other particles within this region, i.e. the contribution from particles with separation $\boldsymbol{x}$ such that $x = O(\Lambda)$ and $y, z = O(L)$, can be calculated as follows. The velocity in the y-direction induced by one particle in the region is $O(\Gamma^{-1}L^{-1})$. Hence, the total velocity fluctuation V_Λ in the y-direction induced by the $O(\Lambda L^2)$ particles in the region, assuming that there are many such particles ($\Lambda L^2 \gg 1$), is given by adding the $O(\Gamma^{-1}L^{-1})$ random velocity fluctuations from each particle to obtain a total variance $V_\Lambda^2 \sim (\Lambda L^2)/(\Gamma L)^2 = \Lambda\Gamma^{-2}$. The total velocity fluctuation V_Λ is expected to persist for the time $T_\Lambda = L/\Lambda$ that it typically takes for the $O(\Lambda)$ shear-velocity difference across the region to change the relative position of the particles by $O(L)$. We expect the random nature of the fluctuations to lead to diffusive growth for $t \gg T_\Lambda$ with a coefficient $D_{yy} \sim V_\Lambda^2 T_\Lambda \sim L\Gamma^{-2}$, which happens to be independent of Λ.

The scaling $D_{yy} \sim L\Gamma^{-2}$ is the same as that of the two-particle diffusivity (5.12). However, in contrast to the two-particle diffusivity, which arises from the ever-decreasing proportion of ballistic displacements that have yet to be reversed, the diffusive growth in this very-long-time regime arises from the more familiar mechanism of a random walk of particle displacements due to repeated unreversed interactions with other particles. The scaling $L\Gamma^{-2}$ is also the same as that suggested by the naive scaling argument in § 4, since the naive argument is simply the above argument with $\Lambda = L$; however, we now understand that L is not the correct choice of Λ since, unless a two-particle interaction is weakly sheared, any horizontal displacement that it causes is mostly reversed at a later time.

The common scaling of the two-particle diffusivity and the very-long-time diffusivity explains why the transition observed in figure 14 is so subtle: the transition simply represents a change in the value of the $O(1)$ coefficient of $L\Gamma^{-2}$. The scaled diffusivities shown in figure 15 suggest that the very-long-time diffusivity is approximately $8 \times 10^{-4} L\Gamma^{-2}$ compared to $9.47 \times 10^{-4} L\Gamma^{-2}$ for the two-particle diffusivity when $S \gg 1$. We note that the scaled values for $L = 5$ are somewhat lower than those for $L \geqslant 10$, perhaps because $L = 5$ is insufficiently large for the assumption $\Lambda L^2 \gg 1$ to hold in the estimate of V_Λ.

We expect the transition to the very-long-time regime to occur when the $O(L/t)$ width of the ballistic region in the two-particle approximation becomes comparable to Λ, which occurs when $t \sim L/\Lambda = T_\Lambda$. Hence, in order to determine the transition time T_Λ, we must determine Λ, which is the range of separations in the x-direction for which the path of one particle relative to another is not well approximated by a vertical straight line. This occurs when the perturbation to the separation between two particles in the x-direction, due to hydrodynamic interactions with other particles, is comparable to their initial separation in the x-direction. Perturbations to the separation in the x-direction can be divided into two groups: relatively large perturbations due

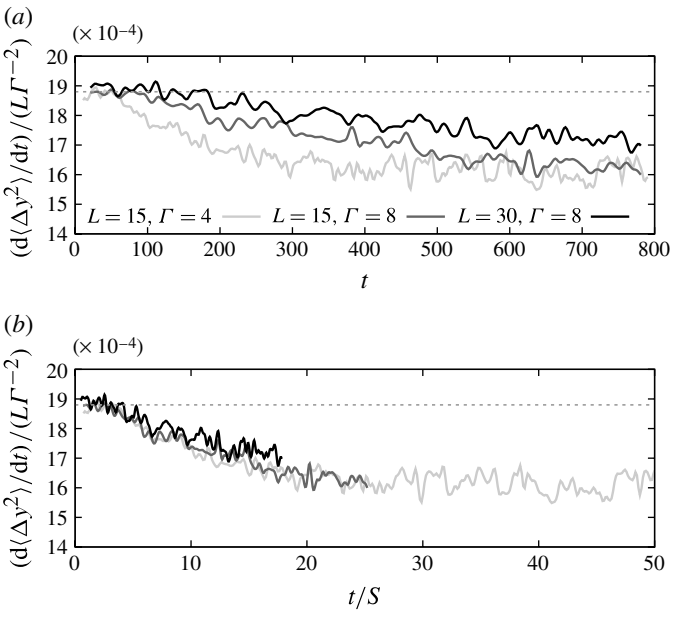

FIGURE 16. Comparison of the local gradient of the (scaled) mean-square displacement for $L = 15$ and $\Gamma = 4$ (grey solid line) as shown in figure 14(*b*) with those for $L = 15$ and $\Gamma = 8$ (dark grey solid line) and $L = 30$ and $\Gamma = 8$ (black solid line). The asymptotic gradient 1.89×10^{-3} predicted by the two-particle approximation (5.26) (dashed grey line) is also shown. (*a*) Gradient plotted against shear time t, and (*b*) gradient plotted against a scaled time of t/S.

to the system-scale hydrodynamic velocity fluctuations, the majority of which are subsequently reversed and thus do not lead to continued growth; and unreversed perturbations, which lead to a very slow diffusive growth as discussed in § 6.1. The reversed perturbations have an $O(L^{1/2}\Gamma^{-1})$ magnitude arising from the $O(L^{1/2}\Gamma^{-1})$ system-scale velocity fluctuations which vary on the $O(1)$ shear time scale. For comparison, the diffusive growth due to unreversed perturbations in the period up to T_Λ has an $O[(D_{xx}T_\Lambda)^{1/2}]$ magnitude, and we recall from (6.6) that D_{xx} decays rapidly as Γ increases. Then, assuming that the $O(L^{1/2}\Gamma^{-1})$ reversed perturbations are the larger of the two contributions, we deduce that $\Lambda \sim L^{1/2}\Gamma^{-1}$ and, consequently, that $T_\Lambda \sim L^{1/2}\Gamma = S$. This scaling of T_Λ, combined with the scaling (6.6) for D_{xx}, confirms that the reversed perturbations are indeed the larger of the two contributions.

The prediction of an $O(S)$ time scale for transition to the very-long-time regime is consistent both with the convergence of diffusion coefficients calculated up to a fixed shear time onto the two-particle diffusivity prediction as $S \to \infty$ (figure 8*b*), and with the different values of the coefficients obtained from a later period when $t \gg S$ (figure 15). The transitions for $L = 15$ and $\Gamma = 4$, for $L = 15$ and $\Gamma = 8$, and for $L = 30$ and $\Gamma = 8$ visualized by changes in the local gradient of the mean-square displacement, are compared in figure 16. Figure 16(*a*) shows that, with $L = 15$, the transition for $\Gamma = 8$ occurs at a later shear time than that for $\Gamma = 4$; and that, with $\Gamma = 8$, the transition for $L = 30$ occurs at a later shear time than that for $L = 15$. The apparent collapse of the three curves when plotted against a scaled time of t/S in figure 16(*b*) supports the argument that $T_\Lambda \sim S$. (Calculation of the gradient of the

mean-square displacement over the long transition period with only a small amount of statistical noise, as in figure 16, is computationally very expensive.)

7. Conclusion

Viscous sedimentation of a suspension of monodisperse point particles in a vertically sheared periodic domain is arguably the simplest example of sedimentation in the presence of a background flow. However, even this simple example exhibits a range of surprising and subtle behaviours.

We have investigated the growth of mean-square particle displacements due to hydrodynamic interactions via numerical simulations with a range of background shear strengths and system sizes. The numerical simulations demonstrated that the horizontal diffusion coefficients decrease as the background shear strength increases, and they revealed a marked contrast between the velocity-gradient and vorticity directions, with diffusion coefficients in the velocity-gradient direction decreasing much more rapidly.

A simple scaling argument shows that the effect of a background shear flow on hydrodynamic diffusion becomes significant when the shear velocity is comparable to hydrodynamic velocity fluctuations on the scale of the system, at which point the shear flow, rather than convective motions driven by the density fluctuations, limits the correlation time of any fluctuations. For strongly sheared systems, where the system-scale shear flow is large compared to the hydrodynamic velocity fluctuations ($S \gg 1$, or $\dot{\gamma} \gg n^{1/2}(f/\mu)\widehat{L}^{-1/2}$ in dimensional terms), it was possible to approximate the horizontal mean-square displacements by considering only two-particle interactions.

In the velocity-gradient direction (x-direction), a numerical calculation showed that, after a transient, the mean-square displacement due only to two-particle interactions asymptotes to a constant value. The absence of any long-term asymptotic growth is due to the symmetry of two-particle interactions in a vertical shear flow and the consequent lack of net horizontal displacements. A scaling argument based on three-particle interactions, which break the symmetry of two-particle interactions by perturbing the separation of the two particles, predicts a dimensional diffusion coefficient of the form

$$\widehat{D}_{xx} \sim \alpha n^2 \left(\frac{f}{\mu}\right)^4 \dot{\gamma}^{-3} \ln\left(\tilde{\beta}\widehat{L}\left(\frac{\mu\dot{\gamma}}{f}\right)^{1/2}\right), \tag{7.1}$$

provided the shear flow is strong compared to the hydrodynamic velocity due to a particle at the typical inter-particle separation ($\Gamma \gg 1$, or $\dot{\gamma} \gg n^{2/3}(f/\mu)$ in dimensional terms). Comparison with numerical simulations showed very good agreement with the predicted scaling and determined the numerical coefficients in the above expression to be $\alpha = 4.2 \times 10^{-4}$ and $\tilde{\beta} = 0.42$.

In the vorticity direction (y-direction), a numerical calculation showed that the mean-square displacement due only to two-particle interactions has an asymptotic diffusion-like linear growth, with a dimensional diffusion coefficient

$$\widehat{D}_{yy} \sim 9.47 \times 10^{-4} n \left(\frac{f}{\mu}\right)^2 \widehat{L}\,\dot{\gamma}^{-1}. \tag{7.2}$$

The growth of the mean-square displacements occurs despite two-particle interactions causing no net displacement. It was shown to originate from displacements due to the weakly sheared two-particle interactions where the two particles are at a similar position in the velocity-gradient direction. Those particles that are separated by only

an $O(L/t)$ distance in the velocity-gradient direction have only undergone a fraction of their interaction by time t and, consequently, their effects are not yet limited by the lack of a net displacement from the full interaction. The $O(t^2)$ ballistic growth of these square displacements combines with the $O(L/t)$ decreasing width of the region of weakly sheared particles to give the observed linear $O(t)$ growth of the mean-square displacements. An asymptotic analysis based on consideration of these weakly sheared particles gave the same diffusivity as the numerically calculated value in (7.2). There is no equivalent effect in the velocity-gradient direction because weakly sheared particles induce much weaker hydrodynamic velocities in that direction.

If diffusion coefficients in the vorticity direction are calculated from a fixed period of shear time, then they converge as S is increased onto the two-particle approximation described above. However, we also found numerical evidence if the shear time becomes very large of a transition into another regime with slightly reduced diffusivity. This transition is associated with the failure of the two-particle approximation when the $O(L/t)$ width of the region contributing to the growth of the mean-square displacements becomes sufficiently narrow, and thus sufficiently weakly sheared, that changes in particle separation are no longer dominated by the shear flow. Beyond this transition, we suggest that the diffusive growth of the mean-square displacements is instead due to unreversed displacements from those interactions for which changes in particle separation are not dominated by the shear flow.

Our original motivation for this study was an improved understanding of hydrodynamic diffusion in sedimenting suspensions with a non-uniform background flow (either imposed or generated by the suspension occupying a spherical or cylindrical region, for example). Although we have only considered a simple system with an imposed uniform vertical shear flow, we can make several observations that ought to be applicable to a wider range of flows. At the most basic level, a background flow introduces new time scales to the system which can influence the time scale on which hydrodynamic velocity fluctuations are correlated. If the background flow is such that two-particle interactions cause no net displacement, then the coefficient of hydrodynamic diffusion could be strongly reduced due to the need for three-particle interactions for any diffusive growth to occur (as seen with D_{xx} in our system). Also, if some regions of the flow remain approximately stationary relative to other regions, then those regions could contribute significantly to hydrodynamic diffusion (as seen with the contribution to D_{yy} from the region of weakly sheared particles in vertical shear). More generally, we note that the long-range nature of hydrodynamic interactions implies that the large-scale structure of the sedimenting suspension is likely to be important in determining hydrodynamic diffusion. As such, it seems unlikely that general results can be obtained for a wide range of systems, but rather that each system must be considered individually.

Acknowledgements

We thank D. Saintillan for bringing to our attention the smooth particle-mesh Ewald method that we implemented for our numerical calculations. A.C. is grateful for support from an EPSRC studentship.

Appendix A. Analysis of two-particle interactions in a periodic system

In § 5, we analysed the mean-square displacements due to two-particle interactions under a quasi-periodic approximation. Here, we perform a similar analysis for the fully periodic system. This requires a suitable method for decomposing the

periodic hydrodynamic velocities. Hasimoto (1959) found the flow due to a triply periodic Stokeslet by Fourier-decomposing the forcing and resulting flow in all three spatially periodic directions. However, for a sheared system, the inverse lattice vectors associated with this decomposition are time-dependent. It is thus simpler to consider the triply periodic Stokeslet as a sum of doubly periodic Stokeslets at different positions x, each of which is periodic in the y–z plane, for which the two-dimensional inverse lattice vectors are time-independent. The solution for a doubly periodic Stokeslet was calculated by Ishii (1979); we only require the result for a square lattice with forcing along one of the periodic directions, which we briefly rederive here in a more concise form.

A.1. *Doubly periodic Stokeslet*

Consider a fluid (with unit viscosity) in an unbounded domain with forcing $\boldsymbol{f}(\boldsymbol{x})$ due to a sheet of sinusoidally varying buoyancy in the plane $x = 0$:

$$\boldsymbol{f}(\boldsymbol{x}) = \exp(\mathrm{i}ly + \mathrm{i}mz)\delta(x)\boldsymbol{e}_z. \tag{A 1}$$

The solution to the Stokes equations for this forcing, with l and m not both zero, can be calculated analytically (e.g. via the Papkovich–Neuber solution) to give

$$\boldsymbol{u}(\boldsymbol{x}) = \hat{\boldsymbol{u}}_{lm}(x)\exp\left(\mathrm{i}ly + \mathrm{i}mz - \sqrt{l^2+m^2}|x|\right) \tag{A 2}$$

and

$$p(\boldsymbol{x}) = \frac{-\mathrm{i}m}{2\sqrt{l^2+m^2}}\exp\left(\mathrm{i}ly + \mathrm{i}mz - \sqrt{l^2+m^2}|x|\right), \tag{A 3}$$

where

$$\hat{\boldsymbol{u}}_{lm}(x) = \frac{-m}{4(l^2+m^2)}\begin{pmatrix}\mathrm{i}\sqrt{l^2+m^2}x\\ l|x|\\ m|x|\end{pmatrix} + \frac{1}{4(l^2+m^2)^{3/2}}\begin{pmatrix}0\\ -lm\\ 2l^2+m^2\end{pmatrix}. \tag{A 4}$$

For convenience, we also define

$$\tilde{\boldsymbol{u}}_{lm}(x) \equiv \exp\left(-\sqrt{l^2+m^2}|x|\right)\hat{\boldsymbol{u}}_{lm}(x), \tag{A 5}$$

which captures all of the variation of $\boldsymbol{u}(\boldsymbol{x})$ with x.

The mode $l = m = 0$, which represents spatially uniform buoyancy, must be treated separately and has solution

$$\boldsymbol{u}(\boldsymbol{x}) = \left(-\frac{|x|}{2} + c\right)\boldsymbol{e}_z. \tag{A 6}$$

This solution has an undetermined constant c and, since the buoyancy force is unbalanced, cannot be matched onto a condition of zero flow at $x = \pm\infty$. In a triply periodic system, the buoyancy due to such modes is balanced by a global pressure gradient. For our present purposes, it is sufficient to note that this mode produces no velocity component in the horizontal directions.

The forcing due to a vertically directed, doubly periodic Stokeslet in the plane $x = 0$ is given by

$$\boldsymbol{f}(\boldsymbol{x}) = \sum_{\boldsymbol{q}}\delta(\boldsymbol{x}-\boldsymbol{q})\boldsymbol{e}_z, \tag{A 7}$$

where the values of $\boldsymbol{q}$ are the lattice vectors in the y–z plane. For a square grid of unit length, the lattice vectors are given by $\boldsymbol{q} = n_y\boldsymbol{e}_y + n_z\boldsymbol{e}_z$ with $(n_y, n_z) \in \mathbb{Z}^2$. In this case, Fourier decomposition of the forcing gives

$$\boldsymbol{f}(\boldsymbol{x}) = \sum_{l,m} \exp(\mathrm{i}ly + \mathrm{i}mz)\delta(x)\boldsymbol{e}_z, \tag{A 8}$$

where $(l, m) \in 2\pi\mathbb{Z}^2$ are inverse lattice vectors. The linearity of the Stokes equations implies that the velocity due to this forcing is simply the forcing due to each of the modes in the sum. Thus, using the above results for the velocity due to a single mode, the horizontal components of the velocity induced at $\boldsymbol{x}$ by such a doubly periodic Stokeslet are

$$\boldsymbol{u}^{d\,H}(\boldsymbol{x}) = \sum_{l} \sum_{m\neq 0} \exp(\mathrm{i}ly + \mathrm{i}mz)\tilde{\boldsymbol{u}}_{lm}(x), \tag{A 9}$$

where modes with $m = 0$ are excluded since they give rise to no horizontal velocity component.

We can reconstruct the horizontal velocities due to a triply periodic Stokeslet as a sum over the x-direction of doubly periodic Stokeslets with z offsets suitably adjusted to take account of advection by the background shear flow:

$$\boldsymbol{u}^{p\,H}(\boldsymbol{x}, t) = \sum_{n} \sum_{l} \sum_{m\neq 0} \exp\{\mathrm{i}ly + \mathrm{i}m(z - nt)\}\tilde{\boldsymbol{u}}_{lm}(x - n), \tag{A 10}$$

with $n \in \mathbb{Z}$.

A.2. *Two-particle displacements*

From (5.7) and (A 10), the horizontal two-particle displacement, $\boldsymbol{X}_1^H(\boldsymbol{x}, t)$, due to a particle at initial separation $\boldsymbol{x}$, can be calculated as

$$\begin{aligned}\boldsymbol{X}_1^H(\boldsymbol{x}, t) = \sum_{n} \sum_{l} \sum_{m\neq 0} \frac{1}{\mathrm{i}m(x - n)} &(\exp\{\mathrm{i}ly + \mathrm{i}m[z + t(x - n)]\} \\ &- \exp\{\mathrm{i}ly + \mathrm{i}mz\})\tilde{\boldsymbol{u}}_{lm}(x - n).\end{aligned} \tag{A 11}$$

Then (5.11) and (A 11) imply that the ensemble-averaged two-particle displacements satisfy

$$\begin{aligned}\langle \boldsymbol{x}^{1H}(t)^2\rangle = \sum_{n} \sum_{l} \sum_{m\neq 0} \int_{-\infty}^{\infty} &\frac{L}{m^2 x(x - n)} \\ &\times (\exp\{\mathrm{i}mtx\} - 1)(\exp\{-\mathrm{i}mt(x - n)\} - 1)\tilde{\boldsymbol{u}}_{lm}(x)\tilde{\boldsymbol{u}}_{-l-m}(x - n)\,\mathrm{d}x.\end{aligned} \tag{A 12}$$

We are now in a position to rederive the results of § 5.4, but for the fully periodic system. To check whether unbounded growth is possible, we consider the time-averaged displacements

$$\langle \overline{\boldsymbol{x}^{1H}(t)^2}\rangle = \sum_{l} \sum_{m\neq 0} \int_{-\infty}^{\infty} \frac{2L}{m^2 x^2}\tilde{\boldsymbol{u}}_{lm}(x)\tilde{\boldsymbol{u}}_{-l-m}(x)\,\mathrm{d}x. \tag{A 13}$$

For the x-direction, this integral is finite and

$$\langle \overline{x^1(t)^2}\rangle = \sum_{l} \sum_{m\neq 0} \int_{0}^{\infty} \frac{L}{4(l^2 + m^2)} \exp\left(-2x\sqrt{l^2 + m^2}\right)\,\mathrm{d}x$$

$$= \sum_{l} \sum_{m \neq 0} \frac{L}{8(l^2 + m^2)^{3/2}}$$

$$= 3.34 \times 10^{-3} L. \tag{A 14}$$

This is consistent with the numerical evolution of the time-dependent problem (figure 6), which found that $\overline{\langle x^1(t)^2 \rangle}$ converged to a constant value of $3.35 \times 10^{-3} L$.

From (A 13), $\overline{\langle y^1(t)^2 \rangle}$ is unbounded, since $\tilde{v}_{lm}(x)$ tends to a constant value as $x \to 0$, leading to a divergent $1/x^2$ factor in the integrand. This is the divergent contribution from weakly sheared two-particle interactions as discussed in § 5.4.

Following § 5.4, we determine the asymptotic behaviour of $\langle y^1(t)^2 \rangle$ by considering the contribution from weakly sheared particles ($x \ll 1$), which dominates (A 12) at long times ($t \gg 1$). In the region where $x \ll 1$, the dominant contribution is from the mode $n = 0$, and $\tilde{v}_{lm}(x)$ can be approximated by its value at $x = 0$. Excluding modes with $n \neq 0$, and making this approximation for $\tilde{v}_{lm}(x)$, gives a long-time asymptotic behaviour of

$$\langle y^1(t)^2 \rangle \sim \sum_{l} \sum_{m \neq 0} \int_{-\infty}^{\infty} \frac{l^2 m^2 L}{8(l^2 + m^2)^3 x^2} (1 - \cos(mtx)) \, \mathrm{d}x. \tag{A 15}$$

To evaluate the integral we make the substitution $mtx = \phi$ to obtain

$$\langle y^1(t)^2 \rangle \sim Lt \sum_{l} \sum_{m \neq 0} \left(\frac{l^2 |m|}{8(l^2 + m^2)^3} \right) \int_{-\infty}^{\infty} \frac{1}{\phi^2} (1 - \cos(\phi)) \, \mathrm{d}\phi$$

$$\sim Lt \sum_{l} \sum_{m \neq 0} \left(\frac{\pi l^2 |m|}{8(l^2 + m^2)^3} \right)$$

$$\sim 1.89 \times 10^{-3} Lt. \tag{A 16}$$

Thus the mean-square displacement in the y-direction due to two-particle interactions exhibits asymptotic linear growth. From (2.10) and (5.9), the implied diffusion coefficient is $D_{yy} \sim 9.47 \times 10^{-4} L \Gamma^{-2}$.

Appendix B. A note on the neglect of finite-size effects

In this appendix, we consider the conditions under which it is appropriate to approximate a suspension of finite-size particles by point particles.

Suppose that the particles occupy a volume fraction ϕ so that their dimensionless size is of order $\phi^{1/3}$. The strain due to the background shear flow will induce a stresslet on each particle, as will hydrodynamic interactions with other particles (with additional higher-order multipole corrections). These stresslets generate velocities that add to the Stokeslet velocities due to the net force on each particle, and affect the particle interactions.

Consider the interaction between a pair of particles with size $\phi^{1/3}$ and separation r. Each particle generates at the other a Stokeslet velocity of order $\Gamma^{-1} r^{-1}$, a stresslet velocity due to the background shear of order ϕr^{-2}, and a stresslet velocity due to hydrodynamic interactions of order $\phi \Gamma^{-1} r^{-4}$. At large separations the Stokeslet velocity will dominate, and at small separations the stresslet velocity (and the higher-order corrections) due to hydrodynamic interactions will dominate. If $\phi \gg \Gamma^{-3/2}$, then there is a regime at intermediate separations where the stresslet velocity induced by

the background shear dominates. However, if $\phi \ll \Gamma^{-3/2}$, then the stresslets due to the background shear flow can be neglected at all separations. Now consider this case.

On scales that are large compared to the particle size ($r \gg \phi^{1/3}$), the Stokeslet velocity is dominant as in the point-particle approximation. On the scale of the particle ($r \sim \phi^{1/3}$), the Stokeslet velocity $\Gamma^{-1}r^{-1}$ and the stresslet velocity $\phi\Gamma^{-1}r^{-4}$ are comparable, and the finite particle size has an effect on the dynamics. The neglect of finite-size effects is appropriate provided such small scales do not make a significant contribution to hydrodynamic diffusion. Since the smallest length scale that we found to contribute to hydrodynamic diffusion in our analysis was $\Gamma^{-1/2}$ (which was the lower limit of contributions to D_{xx}), we expect the neglect of finite-size effects to be appropriate provided that $\phi^{1/3} \ll \Gamma^{-1/2}$.

The conditions on ϕ in the preceding two paragraphs are in fact equivalent, and imply that the neglect of finite-size effects is appropriate provided simply that the shear strength is not too large $\Gamma \ll \phi^{-2/3}$, or $\dot{\gamma} \ll (n/\phi)^{2/3}(f/\mu)$ in dimensional terms.

REFERENCES

ACRIVOS, A., BATCHELOR, G. K., HINCH, E. J., KOCH, D. L. & MAURI, R. 1992 Longitudinal shear-induced diffusion of spheres in a dilute suspension. *J. Fluid Mech.* **240**, 651–657.

BATCHELOR, G. K. 1972 Sedimentation in a dilute dispersion of spheres. *J. Fluid Mech.* **52** (2), 245–268.

BOYCOTT, A. E. 1920 Sedimentation of blood corpuscles. *Nature* **104** (2621), 532.

CAFLISCH, R. E. & LUKE, J. H. C. 1985 Variance in the sedimentation speed of a suspension. *Phys. Fluids* **28** (3), 759–760.

CROSBY, A. & LISTER, J. R. 2012 Falling plumes of point particles in viscous fluid. *Phys. Fluids* **24** (12), 123101.

CUNHA, F. R., ABADE, G. C., SOUSA, A. J. & HINCH, E. J. 2002 Modeling and direct simulation of velocity fluctuations and particle-velocity correlations in sedimentation. *Trans. ASME: J. Fluids Engng* **124** (4), 957–968.

DAVIS, R. H. & HASSEN, M. A. 1988 Spreading of the interface at the top of a slightly polydisperse sedimenting suspension. *J. Fluid Mech.* **196**, 107–134.

ECKSTEIN, E. C., BAILEY, D. G. & SHAPIRO, A. H. 1977 Self-diffusion of particles in shear flow of a suspension. *J. Fluid Mech.* **79** (1), 191–208.

EKIEL-JEŻEWSKA, M. L., METZGER, B. & GUAZZELLI, E. 2006 Spherical cloud of point particles falling in a viscous fluid. *Phys. Fluids* **18** (3), 038104.

GUAZZELLI, E. & HINCH, J. 2011 Fluctuations and instability in sedimentation. *Annu. Rev. Fluid Mech.* **43**, 97–116.

HAM, J. M. & HOMSY, G. M. 1988 Hindered settling and hydrodynamic dispersion in quiescent sedimenting suspensions. *Intl J. Multiphase Flow* **14** (5), 533–546.

HASIMOTO, H. 1959 On the periodic fundamental solutions of the Stokes equations and their application to viscous flow past a cubic array of spheres. *J. Fluid Mech.* **5** (2), 317–328.

ISHII, K. 1979 Viscous flow past multiple planar arrays of small spheres. *J. Phys. Soc. Japan* **46** (2), 675–680.

KERR, R. C., LISTER, J. R. & MÉRIAUX, C. 2008 Effect of thermal diffusion on the stability of strongly tilted mantle plume tails. *J. Geophys. Res.* **113**, B09401.

KOCH, D. L. 1994 Hydrodynamic diffusion in a suspension of sedimenting point particles with periodic boundary conditions. *Phys. Fluids* **6** (9), 2894–2900.

KOCH, D. L. & SHAQFEH, E. S. G. 1991 Screening in sedimenting suspensions. *J. Fluid Mech.* **224**, 275–303.

LADD, A. J. C. 1993 Dynamical simulations of sedimenting spheres. *Phys. Fluids* A **5** (2), 299–310.

LISTER, J. R., KERR, R. C., RUSSELL, N. J. & CROSBY, A. 2011 Rayleigh–Taylor instability of an inclined buoyant viscous cylinder. *J. Fluid Mech.* **671**, 313–338.

MACHU, G., MEILE, W., NITSCHE, L. C. & SCHAFLINGER, U. 2001 Coalescence, torus formation and breakup of sedimenting drops: experiments and computer simulations. *J. Fluid Mech.* **447**, 299–336.

METZGER, B., NICOLAS, M. & GUAZZELLI, E. 2007 Falling clouds of particles in viscous fluids. *J. Fluid Mech.* **580**, 283–301.

MUCHA, P. J. & BRENNER, M. P. 2003 Diffusivities and front propagation in sedimentation. *Phys. Fluids* **15** (5), 1305–1313.

NICOLAI, H. & GUAZZELLI, E. 1995 Effect of the vessel size on the hydrodynamic diffusion of sedimenting spheres. *Phys. Fluids* **7** (1), 3–5.

NICOLAI, H., HERZHAFT, B., HINCH, E. J., OGER, L. & GUAZZELLI, E. 1995 Particle velocity fluctuations and hydrodynamic self-diffusion of sedimenting non-Brownian spheres. *Phys. Fluids* **7**, 12–23.

NITSCHE, J. M. & BATCHELOR, G. K. 1997 Break-up of a falling drop containing dispersed particles. *J. Fluid Mech.* **340**, 161–175.

PIGNATEL, F., NICOLAS, M., GUAZZELLI, E. & SAINTILLAN, D. 2009 Falling jets of particles in viscous fluids. *Phys. Fluids* **21** (12), 123303.

SAINTILLAN, D., DARVE, E. & SHAQFEH, E. S. G. 2005 A smooth particle-mesh Ewald algorithm for Stokes suspension simulations: the sedimentation of fibres. *Phys. Fluids* **17** (3), 033301.

SIEROU, A. & BRADY, J. F. 2004 Shear-induced self-diffusion in non-colloidal suspensions. *J. Fluid Mech.* **506**, 285–314.

SMOLUCHOWSKI, M. S. 1913 On the practical applicability of Stokes' law of resistance, and the modifications of it required in certain cases. In *Proceedings of the Fifth International Congress of Mathematicians*, vol. II. pp. 192–201. Cambridge University Press.